

See discussions, stats, and author profiles for this publication at: <https://www.researchgate.net/publication/330876003>

# Crustal structure across the Lord Howe Rise, northern Zealandia, and rifting of the eastern Gondwana margin

Article in *Journal of Geophysical Research: Solid Earth* · February 2019

DOI: 10.1029/2018JB016798

---

CITATION

1

READS

11

8 authors, including:



Flora Gallais

Institut Français des Sciences et Technologies des Transports, de l'Aménagement et ...

22 PUBLICATIONS 127 CITATIONS

[SEE PROFILE](#)



Brian Boston

Japan Agency for Marine-Earth Science Technology

24 PUBLICATIONS 95 CITATIONS

[SEE PROFILE](#)



Seiichi Miura

Japan Agency for Marine-Earth Science Technology

83 PUBLICATIONS 1,496 CITATIONS

[SEE PROFILE](#)



## RESEARCH ARTICLE

10.1029/2018JB016798

This article is a companion to Boston et al. (2019), <https://doi.org/10.1029/2018JB016799>.

**Key Points:**

- The Lord Howe Rise and Dampier Ridge are thinned Zealandia continental fragments separated by oceanic crust in the Middleton Basin
- There is no evidence for mantle exhumation or high-velocity igneous intrusive bodies during rifting and breakup of eastern Gondwana
- Despite the width and magma-poor nature of northwestern Zealandia, it lacks other typical features of a hyperextended continental margin

**Supporting Information:**

- Supporting Information S1

**Correspondence to:**

G. Fujie,  
fujie@jamstec.go.jp

**Citation:**

Gallais, F., Fujie, G., Boston, B., Hackney, R., Kodaira, S., Miura, S., et al. (2019). Crustal structure across the Lord Howe Rise, northern Zealandia, and rifting of the eastern Gondwana margin. *Journal of Geophysical Research: Solid Earth*, 124. <https://doi.org/10.1029/2018JB016798>

Received 29 SEP 2018

Accepted 8 DEC 2018

Accepted article online 4 FEB 2019

©2019. The Authors.

This is an open access article under the terms of the Creative Commons Attribution-NonCommercial-NoDerivs License, which permits use and distribution in any medium, provided the original work is properly cited, the use is non-commercial and no modifications or adaptations are made.

## Crustal Structure Across the Lord Howe Rise, Northern Zealandia, and Rifting of the Eastern Gondwana Margin

Flora Gallais<sup>1</sup>, Gou Fujie<sup>1</sup> , Brian Boston<sup>1</sup> , Ron Hackney<sup>2</sup> , Shuichi Kodaira<sup>1</sup> , Seiichi Miura<sup>1</sup>, Yasuyuki Nakamura<sup>1</sup>, and Yuka Kaiho<sup>1</sup>

<sup>1</sup>Research and Development Center for Earthquake and Tsunami, Japan Agency for Marine-Earth Science and Technology, Yokohama, Japan, <sup>2</sup>Resources Division, Geoscience Australia, Canberra, ACT, Australia

**Abstract** During the Late Cretaceous, the fragmentation of eastern Gondwana led to the formation of the narrow eastern Australian margin and the wide Lord Howe Rise during the opening of the oceanic Tasman Basin. To provide crustal-scale constraints on this margin, a 680-km-long, east-west oriented refraction transect with 100 ocean bottom seismometers was acquired from the Tasman Basin to the Lord Howe Rise. After traveltimes tomographic inversion of the first refracted arrivals and reflected arrivals from the Moho, the final *P* wave velocity model reveals strong variations in crustal thickness. The Tasman Basin is floored by a two-layered and 7-km-thick oceanic crust. To the east, the Middleton Basin separates the Dampier Ridge, with 16-km-thick continental crust, from the Lord Howe Rise, where the extended continental crust is 20–23 km thick. Below the Middleton Basin, Moho reflections are recorded at the base of 7-km-thick crust. The velocity gradient of this two-layer crust suggests an oceanic origin for the Middleton Basin. Our results show no clear evidence for mantle exhumation or a sizable igneous intrusion within three separate and relatively narrow (<70 km) necking zones. The northwestern Zealandia margin thus appears to be magma poor and, despite the considerable width of this margin (>1,000 km), the lack of evidence for mantle exhumation, the evidence for oceanic crust under the Middleton Basin, and the narrow necking zones combine to suggest that northern Zealandia is not a hyperextended margin.

### 1. Introduction

Numerous studies have used wide-angle seismic data to focus on understanding the rifting processes that lead to the formation of passive continental margins (Chian et al., 1999; Dean et al., 2000; Eddy et al., 2018; Funck et al., 2016; van Avendonk et al., 2006). Based on the *P* wave velocity structure and detailed analysis of one-dimensional velocity-depth profiles extracted below the top of basement, the wide-angle profiles are used to identify crustal domains (oceanic, continental, and continent-ocean transition zones) that are defined by crustal thickness and seismic velocity. By characterizing the symmetry of the conjugate margins, the volume of magmatic rocks intruded or underplated, and the absence or presence of exhumed material (lower continental crust or mantle) at the continent-ocean transition, fundamental questions regarding the mechanism of rifting can be addressed (e.g., magmatic versus amagmatic rifting, pure shear versus simple shear extension, or the possibility of depth-dependent stretching; Aslanian et al., 2009; Whitmarsh et al., 2001).

In the southwest Pacific the oceanic Tasman Basin opened as a result of rifting between eastern Australia and the Lord Howe Rise, the geological backbone to northern Zealandia (Figure 1a; Mortimer et al., 2017). Rifting in this region produced large asymmetry of extension in the resulting margins (e.g., Müller et al., 2016). A detachment fault model (Lister et al., 1986, 1991) has been proposed to explain the asymmetry between eastern Australia, an ~50-km-wide margin, and Zealandia, a >1,000-km-wide margin (van de Beuke et al., 2003). However, due to the limited number of seismic refraction studies in the area (Figure 1b), the crustal geometry of the Tasman Basin and the Lord Howe Rise remains poorly constrained and the nature of the crust underlying the Lord Howe and Middleton Basins is still unknown. Motivated by a proposal to the International Ocean Discovery Program (IODP) for deep scientific drilling through a Lord Howe Rise rift basin (IODP Proposal 871-CPP), in 2016 we acquired a 680-km-long wide-angle transect across the Tasman Basin and the Lord Howe Rise to image crustal structure in a region that records the

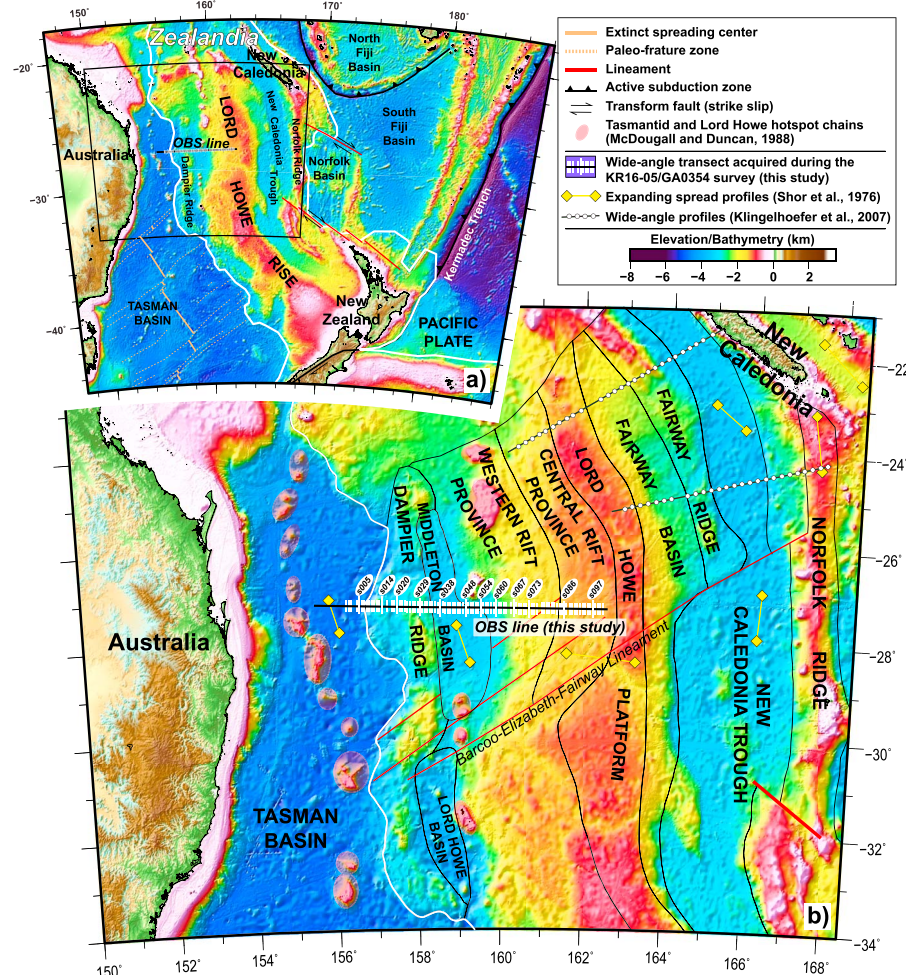


**Figure 1.** (a) Bathymetric map of the SW Pacific region around the studied area (black box) showing the outline (in white) of Zealandia (Mortimer et al., 2017). Extinct seafloor spreading in the Tasman Basin is from Gaina, Müller, et al. (1998); Gaina, Roest, et al. (1998). (b) Bathymetric map of the studied area showing key domains of the northern Lord Howe rise, with the major tectonic boundaries (Collot et al., 2012; Stagg et al., 1999). Positions of the Ocean Bottom Seismometers (OBSs) deployed during the KR16-05/GA0354 survey are shown by the white ticks and the black line shows the air gun shooting. The long white ticks with labels indicate the locations of OBS sections shown in Figure 2. Positions of the previous wide-angle experiments are shown by yellow diamonds and green circles (Klingelhoefer et al., 2007; Shor et al., 1976).

~100-million-year tectonic history of the eastern Gondwana margin. The aim of this study is to determine  $P$  wave crustal velocity across the Tasman Basin to the northern Lord Howe Rise. The final  $P$  wave velocity model is used to describe the main characteristics (crustal thickness, nature of the crust) of these tectonic provinces and to discuss the nature of the crust below the Middleton Basin. Based on these new findings, the geodynamic evolution of eastern Gondwana is reviewed and the processes leading to the opening of the Tasman Basin are discussed.

## 2. Tectonic Setting

Zealandia is a >2,000-km-long and >1,000-km-wide ribbon of extended and mostly submerged continental crust that was a part of eastern Gondwana until the Late Cretaceous (Figure 1; Mortimer et al., 2017). The geodynamic history of this region involved successive tectonic phases of convergence and divergence. During the Triassic and Early Cretaceous, the eastern Gondwana margin was characterized by west/southwest dipping subduction of the oceanic Phoenix-Pacific Plate (Li et al., 2012; Matthews et al., 2015; Müller et al., 2016). Widespread rifting occurred during the Late Cretaceous, leading to the progressive

isolation of the Lord Howe Rise from Australia (Crawford et al., 2002; Gaina, Müller, et al., 1998; Gaina, Roest, et al., 1998; Higgins et al., 2015; Schellart et al., 2006). Limited sampling of basement rocks provides constraints on the extended continent. East of the Tasman Basin, the Dampier Ridge flanks the northern Lord Howe Rise, and this ridge is known to be continental in origin, based on dredging of Permian granitic rocks (McDougall et al., 1994). To the east of the Dampier Ridge, the western side of the Lord Howe Rise is characterized by the presence by numerous rifted basins that have previously been subdivided into Western and Central Rift Provinces based on sediment thickness and structural style (Higgins et al., 2015; Stagg et al., 2002; Willcox et al., 2001). Dredged samples of Triassic-Jurassic granites suggest that the crust underlying these provinces is continental in origin (Mortimer et al., 2015).

Seafloor spreading in the south Tasman Basin started at ~85 Ma (Gaina, Müller, et al., 1998; Gaina, Roest, et al., 1998). The rifting then propagated to the north leading to the opening of the Middleton and Lord Howe Basins during the separation of the Lord Howe Rise from the Dampier Ridge, which was still attached to Australia (Jongsma & Mutter, 1978). The Lord Howe and Middleton Basins are N-S oriented basins that are ~100 km wide and filled by several kilometers of sediments (Stagg et al., 1999; Willcox et al., 2001). However, the nature of the crust underlying the Lord Howe and the Middleton Basins has yet to be constrained. Rifting in the Middleton and Lord Howe Basins ended at 72 Ma and then oblique spreading in the northern Tasman Basin took place until 52 Ma between Australia and the Dampier Ridge (Gaina, Müller, et al., 1998; Gaina, Roest, et al., 1998). The tectonic processes that led to the opening of the oceanic Tasman Basin are still debated but have been linked to plume-ridge interaction (Gaina et al., 2003) potentially related to the Whitsunday Volcanic Province (Bryan et al., 1997) or to easterly directed roll-back of the Gondwana margin subducting slab (Matthews et al., 2015; Müller et al., 2016; Schellart et al., 2006).

Since the breakup of eastern Gondwana, northern Zealandia may have experienced additional convergence on its eastern margin. An Eocene unconformity is proposed to mark a period of rapid subsidence along the New Caledonia Trough that resulted from Paleogene initiation of Tonga-Kermadec subduction (Sutherland et al., 2010). Additionally, the Tasman Basin and the Lord Howe Rise are cross cut by two north-south oriented chains of Miocene and Oligocene volcanoes that were sourced from the Tasmantid and the Lord Howe hotspots (Figure 1b; Dadd et al., 2011; McDougall & Duncan, 1988).

### 3. Data

#### 3.1. Data Acquisition

In 2016, a combined reflection and wide-angle seismic transect was acquired offshore from eastern Australia across the Tasman Basin, the Dampier Ridge, the Middleton Basin, and the western side of the Lord Howe Rise (Figure 1b). The seismic line is oriented east-west and is 680 km long. One hundred Ocean Bottom Seismometers (OBSs) were deployed along the profile at intervals of 6 km, and for OBS recording we fired an air gun array (total volume of 7,800 cubic inches) from the R/V *Kairei* at 200-m intervals. A multichannel seismic reflection (MCS) survey was also conducted along the survey line using a 444-channel hydrophone streamer with a 6-km length and the same air gun array but fired at 50-m intervals. The MCS data provide detailed seismic images of the sedimentary section and underlying crust (Boston et al., 2019).

Each OBS had three-component geophones equipped with gimbal-leveling mechanisms and a hydrophone sensor. The position of each OBS on the seafloor was determined using traveltimes arrivals of the direct water wave within an offset of 5 km recorded by the OBS. During the seismic survey, the OBSs planned for sites s003 and s076 were not deployed due to the proximity to submarine cables and OBSs s013, s015, s017, and s064 were not recovered.

#### 3.2. Arrivals Recorded by the OBSs

As examples of the high-quality recorded sections, Figure 2 shows the recorded refracted phases (refractions from the sediments [Ps], the crust [Pg], and the uppermost mantle [Pn]) and reflected arrivals from the Moho (PmP; see location of the OBSs in Figure 1b). The first-arrived phases are generally apparent at offsets up to 130 km (Figures 2a to 2l). On the OBSs deployed in the Tasman Basin, first-arrived phases interpreted as refractions from the crust and from the uppermost mantle are characterized by apparent velocities of 5.6 and 8 km/s, respectively (Figure 2a). The Pg-Pn crossover offset (distance between shot and receiver where

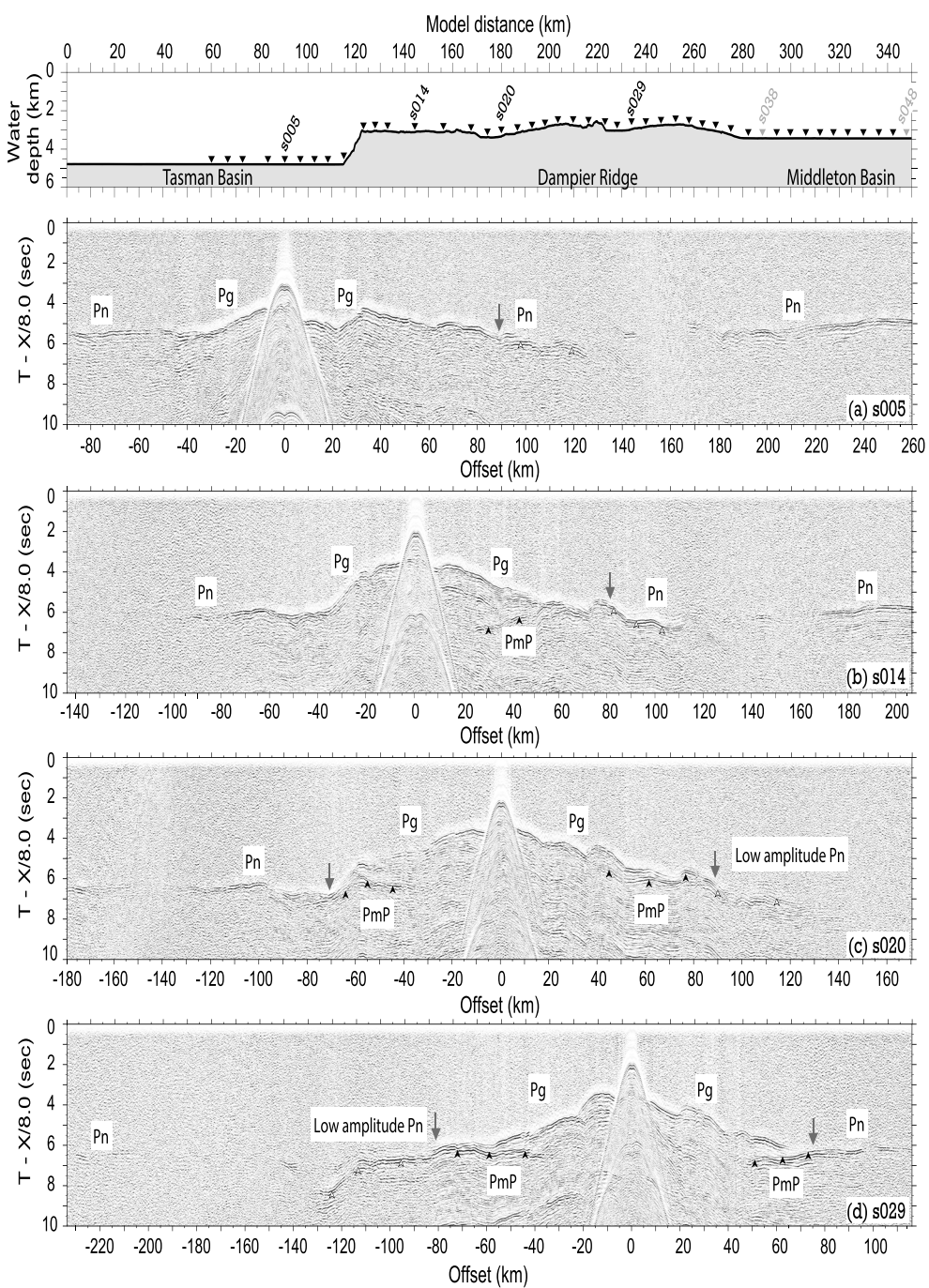


**Figure 2.** Examples of Ocean Bottom Seismometers (OBS) records (vertical component): (a) s005, (b) s014, (c) s020, (d) s029, (e) s038, (f) s048, (g) s054, (h) s060, (i) s067, (j) s073, (k) s086, and (l) s097. Data are band-pass filtered 5–15 Hz and a wiener predictive deconvolution filter with 0.075-s gap and 0.25-s operator length, and 1-s automatic gain control have been applied. The gray arrows show the triplication point between the crustal arrivals (Pg) and arrivals from the mantle (Pn). The reflected arrivals from the Moho are labeled PmP. Ps corresponds to the first arrivals from sediments. The upper panel shows seafloor topography along the profile and the position of the OBSs. Zoomed record sections of the same sites are presented in Figure S1.

Pn becomes a first arrival) increases from 35 km in the Tasman Basin (Figure 2a) to 90 km on the Dampier Ridge (Figures 2b to 2e). This variation suggests large crustal thickness variation between the Tasman Basin and the Dampier Ridge. The later reflected arrivals from the Moho are very sparse below the Tasman Basin.

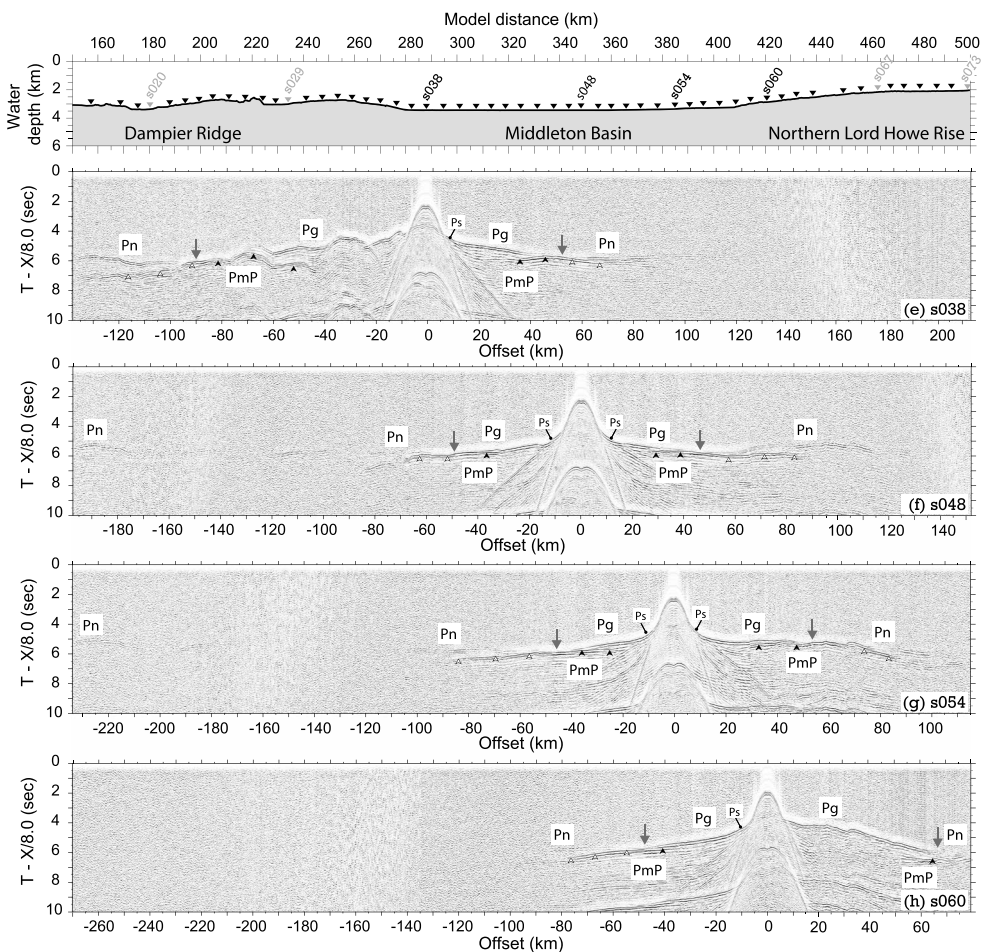


Figure 2. (continued)

The sharp relief of the Dampier Ridge strongly imprinted the data recorded by the OBSs deployed on the Dampier Ridge (Figures 2a and 2d). Below the Dampier Ridge, the Pn refracted phases from the uppermost mantle are recorded and propagate up to large offsets reaching 250 km. The Pn phases are rather continuous, high-amplitude first arrivals with apparent velocities of 8 km/s (Figures 2a to 2c toward the east and Figures 2d to 2g toward the west).

In the Middleton Basin, neighboring OBS record sections vary gradually, so the crustal structure must be laterally continuous on the scale of the OBS spacing (6 km; Figures 2e to 2h). First refracted arrivals (Ps) traveling within the sediments are recorded between offsets of 5 to 15 km (Figures 2e to 2g). The apparent velocity of the Ps arrivals increases gradually from 2.5 to 4.2 km/s (Figures 2e to 2g). At offsets of 15 to ~50 km, the apparent velocity of refracted arrivals from the crust is 7 km/s. The OBSs located in the Middleton Basin recorded very strong precritical and postcritical PmP reflected phases from the Moho and at offsets of up to 80 km (Figures 2e to 2i). The Pn refracted phases are recorded as first arrivals at ~50 km on all the OBSs deployed in the Middleton Basin, suggesting thin crust with constant thickness.

On the extended western margin of the Lord Howe Rise, the refracted arrivals from the sediments are recorded between offsets of 5 to 8–15 km, suggesting variations in sediment thickness (Figures 2i to 2l). The Pg first-arrived from the crust is strongly imprinted by the rough geometry of the top of the basement below these provinces. The Pg-Pn crossover offset ranges from 80 and 100 km, suggesting thicker crust under the western side of the Lord Howe Rise than under the Middleton Basin (Figures 2i to 2l). The PmP reflected from the Moho is characterized by very strong amplitude (Figures 2i to 2l). Below the Western and Central Rift Provinces of the Lord Howe Rise, the amplitude of the Pn is very weak and the Pn is recorded to offsets of up to 120 km (Figures 2i to 2l).

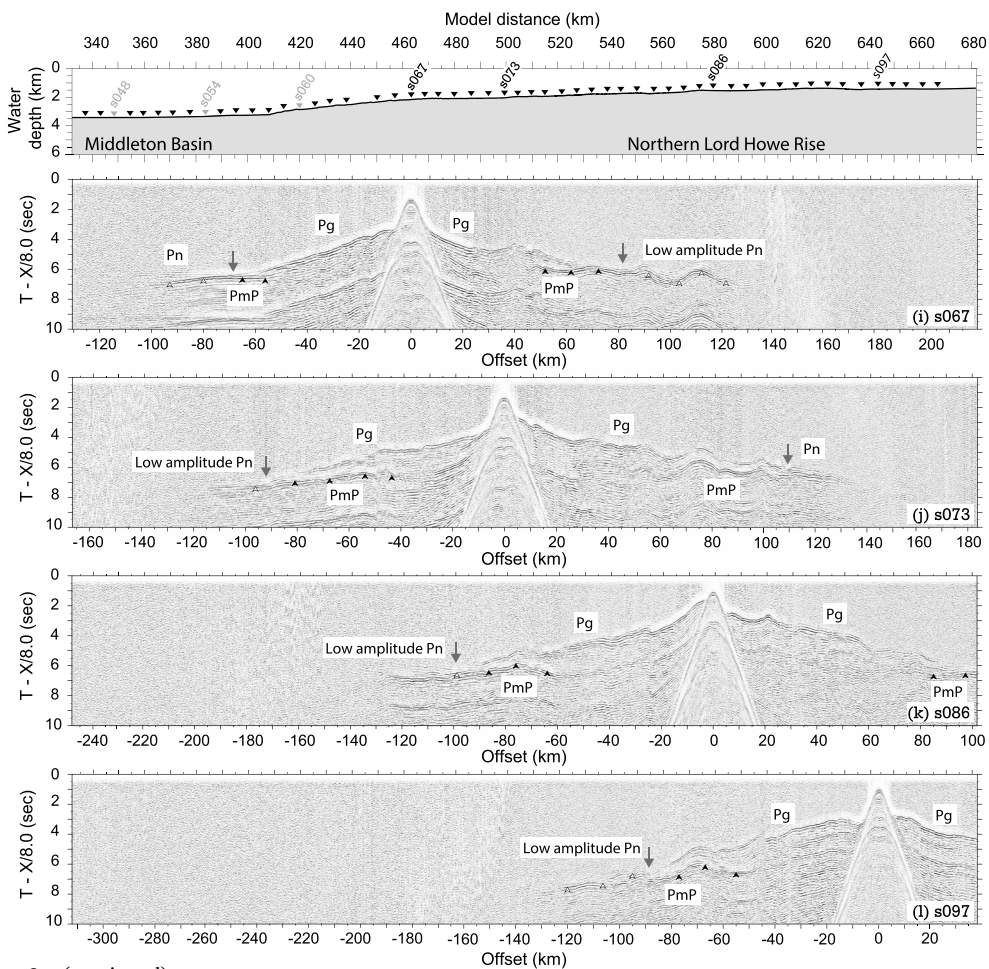
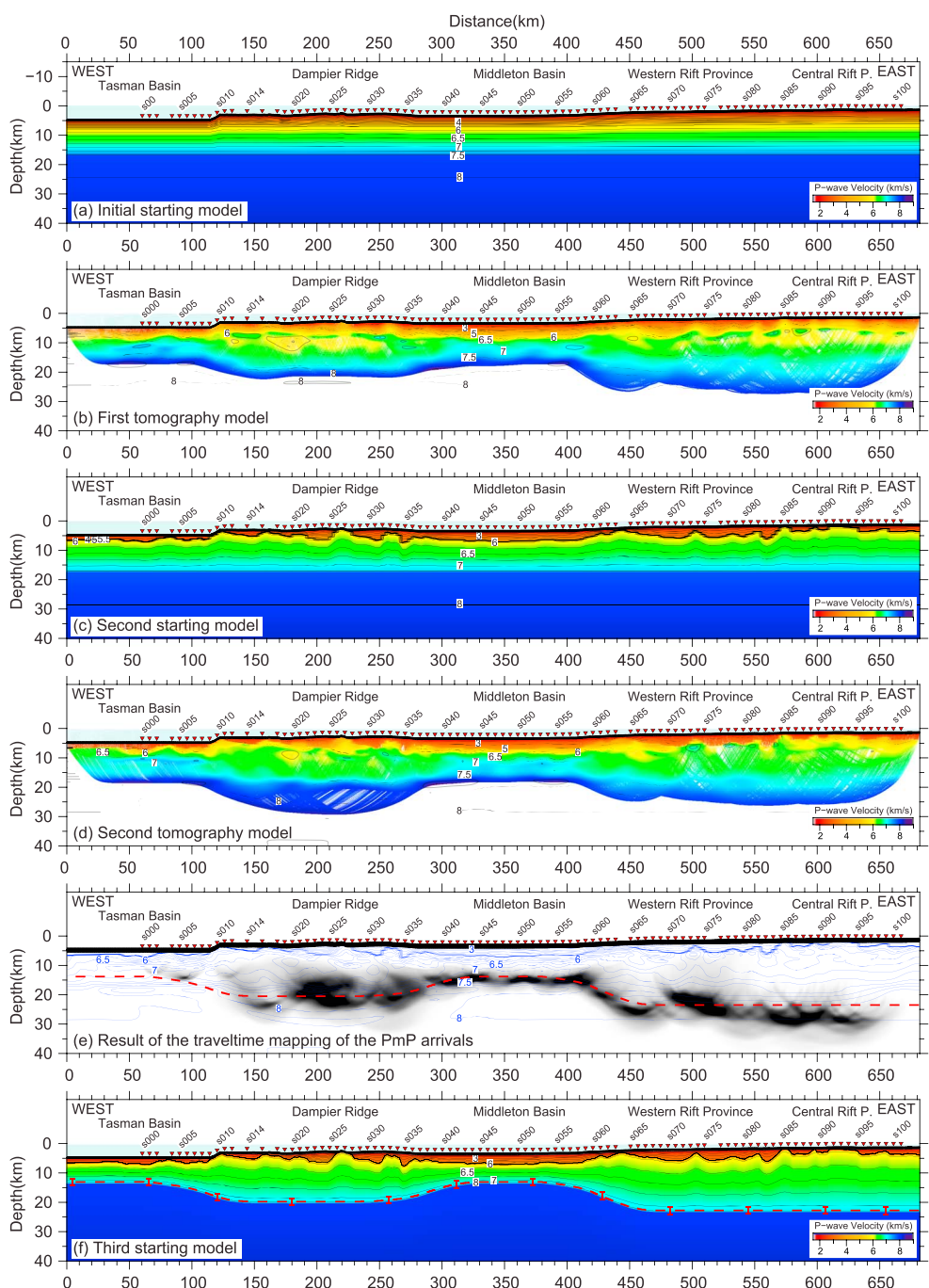


Figure 2. (continued)

#### 4. Traveltime Tomography

We determined a  $P$  wave velocity model using a three step traveltome inversion. First, we applied first arrival tomography (Fujie et al., 2006, 2013). We manually picked a total of 112,086 first arrivals and assigned a picking error ranging from 56 to 217 ms, with the error increasing with the offset of the arrivals. To assess the main characteristic features along the profile, we used an initial  $P$  wave velocity model consisting of two layers (Figure 3a). The top layer is seawater with an assumed uniform velocity of 1.51 km/s. The seafloor topography is extracted from the multibeam bathymetry data acquired during the survey. The second layer corresponds to the sediments with velocities ranging from 1.6 to 5.5 km/s, the crust with velocities ranging from 5.8 to 7.5 km/s, and the mantle with velocities ranging from 7.9 to 8.2 km/s (Figure 3a). The velocity field of the second layer is represented by a regular grid with nodes spaced 3 km horizontally and 0.25 km vertically. During the tomographic inversion, we applied smoothness constraints to stabilize the tomographic velocity field.

Key features evident in the  $P$  wave velocity model from the first traveltome tomography (Figure 3b) include (i) a complex shallow sedimentary structure with numerous basins and basement highs and (ii) large-scale crustal thickness variations along the profile. To better constrain these variations, we ran a second traveltome tomography using an updated starting model incorporating the MCS time-migrated data. On the time-migrated MCS profile, many sedimentary basins are imaged with varying thicknesses and widths (Figure 4a; Boston et al., 2019). The goal of this second-step tomography was to include these sedimentary basins in the starting model to allow the generation of a more realistic traveltome tomography model.



**Figure 3.** Modeling strategy for this study. Vertical exaggeration is 2.5. (a) Initial starting model for the first tomographic inversion and (b) resulting tomography model. (c) Starting model for the second tomographic inversion and (d) resulting tomography model. (e) Mapping of the PmP arrivals recorded by the Ocean Bottom Seismometers (OBSs) using the travelttime mapping method (Fujie et al., 2006). The color density does not show the reflection strength directly but indicates the number of stacked picks. The dashed red line indicates the geometry of Moho used in the parametrization of the third starting model. (f) Starting model for the third and final tomographic inversion. The dashed red line highlights the geometry of the starting Moho from (e) and its associated standard deviation of 2 km.

Based on the MCS time-migrated data, the sedimentary section can be divided as follows: (i) an upper, quasi transparent unit with a relatively constant thickness of 0.5-s twt (two-way travelttime) and (ii) a lower unit of variable thickness that contains well-stratified subunits (Figure 4a). These two main seismic units can be

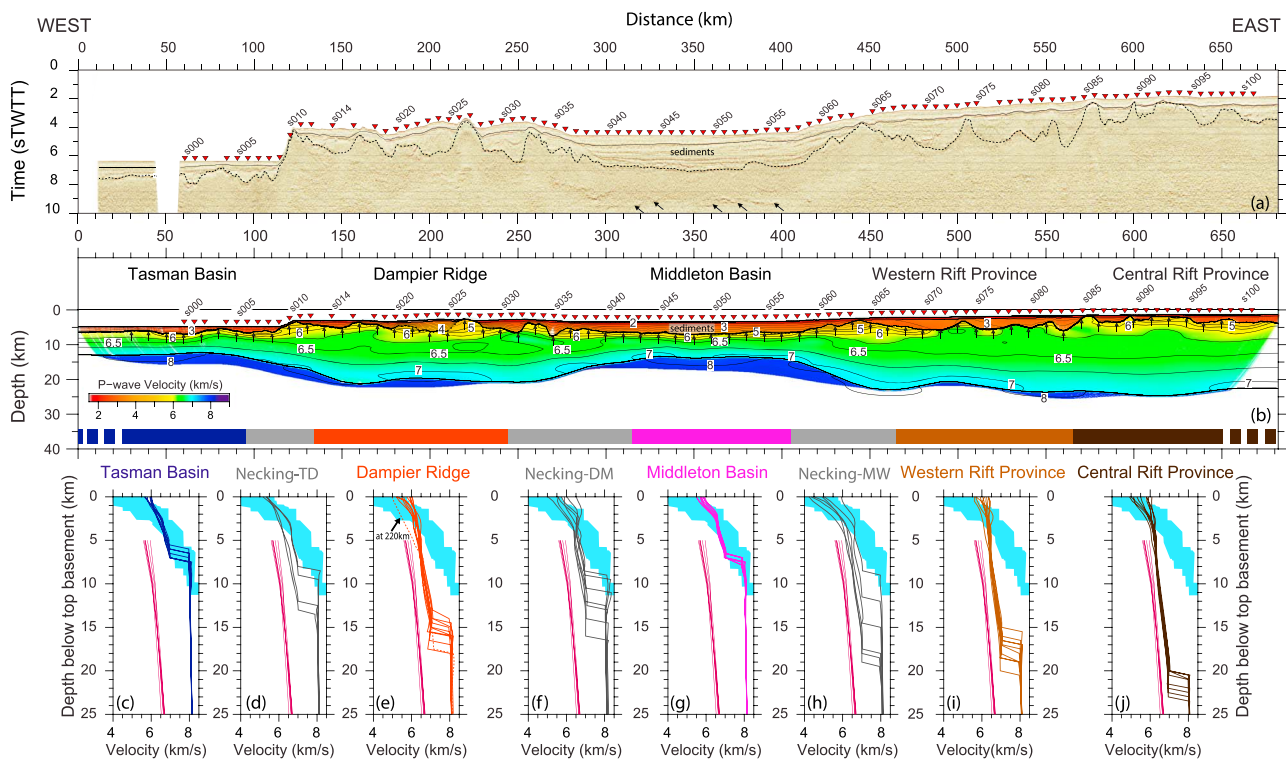


**Figure 4.** (a) Time section showing coincident multichannel seismic reflection (MCS) data along the Ocean Bottom Seismometer (OBS) line (Boston et al., 2019). The top of the basement is shown by the thick black dotted line. The black arrows in the Middleton Basin indicate reflections interpreted to be from the base of the crust. Vertical exaggeration is 10.5. (b) Final  $P$  wave velocity model. Isovelocity contour interval is 0.25 km/s. The black arrows indicate the top of the crystalline crust and the position of the 1-D velocity-depth profiles shown below. Vertical exaggeration is 2. (d to j) 1-D velocity-depth profiles below the base of sediments extracted at 10-km intervals along the profile and, for comparison, velocities for oceanic crust in the Atlantic Ocean (blue shaded area; White et al., 1992) and continental crust (purple lines; Christensen & Mooney, 1995). For the necking zones, the acronyms are TD for Tasman Basin/Dampier ridge, DM for Dampier ridge/Middleton Basin, and MW for Middleton Basin/Western Rift Province.

recognized in the OBS data and are associated with the two main sedimentary arrivals (Figures 2f and 2g): (i) at short offsets (less than 10 km), the first Ps arrivals are characterized by an apparent velocity of 1.9 km/s and (ii) at larger offsets (from 10 to 20–30 km), the Ps arrivals are characterized by increasing apparent velocity that reaches 3.0 to 4.2 km/s. On the MCS time-migrated profile, we picked the horizons at the base of the upper sedimentary unit and at the top of the basement (Figure 4a) and converted to depth for inclusion as interfaces in the starting model (Figure 3c). Based on these constraints, the updated starting model included two sedimentary layers: (i) an upper layer with velocity ranging from 1.6 km/s at the top of the layer to 2.2 km/s at the bottom, with nodes at 3 km spacing, and (ii) a lower sedimentary layer with velocity ranging from 2.5 to 3.0–4.5 km/s, with nodes at 6-km spacing. The underlying fourth layer corresponds to the crust and the mantle, with velocities ranging from 5.8 to 7.1 km/s for the crust and 7.9 to 8.2 km/s for the mantle, and its velocity field is represented on a regular grid with a  $3 \times 0.25$  km spacing. The Moho of the starting model was assumed to be flat and located at a depth of 17 km below sea level (Figure 3c). Using first arrivals picked on the OBS data and two-way reflection traveltimes picked on the MCS time-migrated profile, we computed a second tomographic  $P$  wave velocity model using travelttime inversion (Fujie et al., 2013). In the second tomography model, the  $P$  wave velocity of the sediments and the sediment thicknesses are better constrained. The crustal thickness variations are confirmed but are still poorly defined (Figure 3d).

To model reliable crustal  $P$  wave velocities and the thickness of the crust, we combined the second  $P$  wave velocity model (Figure 3d) with the travelttime mapping method (Fujie et al., 2006). This method allows us to image the geometry of the Moho based on the PmP arrivals recorded by the OBSSs (Figure 3e). We picked 43,625 PmP arrivals with a picking error ranging from 56 to 133 ms. After mapping the reflected

**Table 1***Reduction of the Traveltime Misfit for Each Traveltime Inversion Step*

	Starting model		Final model		Phases	Figure
	RMS (ms)	$\chi^2$	RMS (msec)	$\chi^2$		
First	660.7	80.64	69.3	0.69	first arrivals	3a, 3b
Second	465.1	16.05	77.8	1.04	first arrivals, MCS reflections	3c, 3d
Third	207.8	6.58	87	1.03	first arrivals, MCS reflections, PmP	3f, 4b

*Note.* We applied traveltome inversion three times using different phases and different starting models. In each inversion,  $\chi^2$ , which is the sum of the squared traveltome misfits divided by pick uncertainty, approached 1.0, showing that the traveltome misfits after inversion are comparable to the assigned errors.

PmP arrivals (Figure 3e), we interpreted the geometry of the Moho as a simplified representation of the Moho imaged by the PmP data (red dotted line in Figure 3e). Based on this Moho geometry, we revised the second tomography model to build a five-layer third starting model (Figure 3f). From this third starting model, we obtain the final *P* wave velocity model after six iterations using first arrivals and PmP reflections from the OBS data and two-way reflection traveltimes form the MCS data (Figure 4b). During the iterations, the root-mean-square (RMS) of traveltome misfit decreases from 209.8 to 86.2 ms and the  $\chi^2$  value reaches 1.03 in the final iteration. The RMS of traveltome misfit is summarized in Table 1.

To illustrate the accuracy of the final velocity model (Figure 4b), for each OBS we calculated the residual between observed and calculated traveltimes for the first-arrival phases (Figure 5a), and for the reflected phases from the Moho (Figure 5b). For first-arrival phases, the traveltome residual is small ( $< \pm 0.15$  s) at offsets between 0 and 70 km (Figure 5a). The traveltome residual of the first arrivals increases at greater offsets ( $> 100$  km; Figure 5a), but all the calculated traveltimes fit within the picking error assigned to observed first arrival phases, which increases with the offset of the arrivals. For phases reflected from the Moho, the calculated traveltome residual is between 0 and 0.15 s, except for the PmP arrivals recorded at the eastern edge of the Dampier Ridge (see between 200- and 300-km model distance in Figure 5b). Overall, the residual between observed and calculated traveltimes is small and fits within the uncertainty assigned to the picked first arrivals and PmP phases.

To evaluate the spatial resolution of the final model, we applied a checkerboard resolution test. A synthetic model (Figure 5c) consisting of sinusoidal anomalies with dimensions 30 km horizontally by 7.5 km vertically was superimposed onto the final tomographic velocity model of Figure 4b. The maximum amplitude of velocity perturbations in the synthetic model is  $\pm 5\%$  from the background velocity (Figure 5c). The differences between the synthetic model (Figure 5c) and the inverted model after six iterations are displayed in Figure 5d. The spatial resolution of the final *P* wave velocity model is evaluated by how well the inversion recovered the perturbation pattern using the final tomographic model as the starting model. The anomalies tested (30 km by 7.5 km) are well resolved to 10-km depth and, in the Middleton Basin, to 15-km depth (Figure 5d). Between 10- and 20-km depth, the checkerboard resolution test shows poorer recovery of the initial pattern (Figure 5d). Figure 5e shows calculated ray density. Ray coverage in the final model is very good to 17-km depth below the Middleton Basin and generally to 10-km depth elsewhere in the model. In the Western and Central Rift provinces of the Lord Howe Rise, the ray coverage at depth is sparser (Figure 5e).

Finally, to support the final *P* wave velocity model derived from the first-arrival traveltome tomography (Figure 4b), we performed a Monte Carlo analysis using the do\_inver code (Fujie et al., 2013; see the supporting information for more details on the method). The Monte Carlo analysis assesses (i) the dependency of the final model on the initial model parameterization and (ii) the uncertainty of the final model obtained after the first arrival traveltome tomography. The comparison between the average of the final *P* velocity models obtained after the Monte Carlo analysis (Figure S2c) and the final model resulting from the traveltome tomography (Figure 4b) shows that many similarities exist between these two final models, both in the *P* wave velocity structure of the crust and in the geometry of the Moho. The main discrepancy is for the Moho depth below the Tasman Basin (in particular between 0 and 70 km model distance – Figures 5d and S1c). This discrepancy is due to the absence of strong constraints on the thickness of the crust below

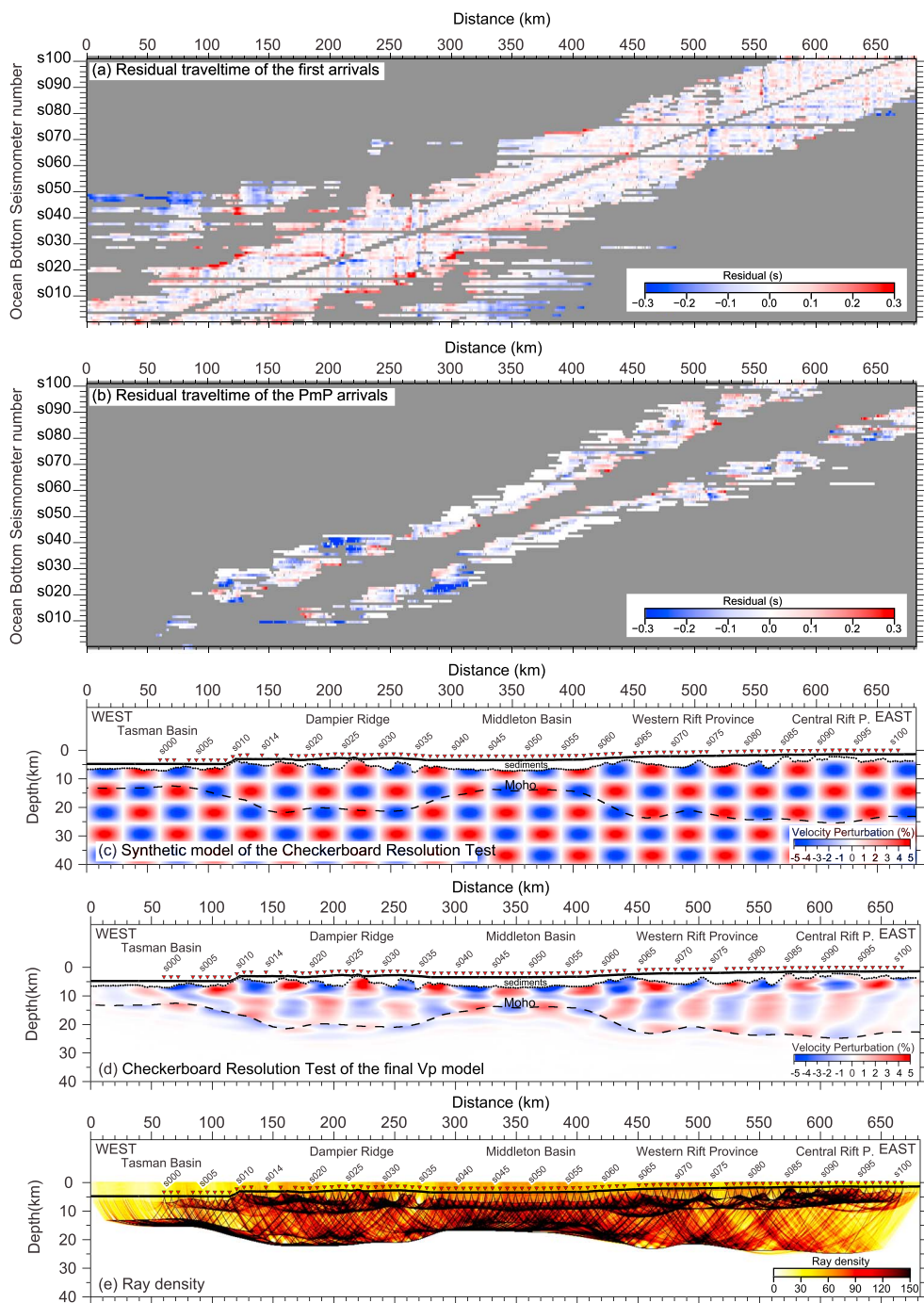


**Figure 5.** Evaluation of the final  $V_p$  model (residual, in seconds, between the observed and calculated traveltime for (a) first arrivals and (b) PmP arrivals; the residuals are for each shot at each Ocean Bottom Seismometer (OBS)). (c) The synthetic model used for the checkerboard resolution test. (d) The results of the resolution test. Ray density in the tomographic model is shown in e. For (c)–(e), the vertical exaggeration is 2.5.

the Tasman Basin arising from the following: (i) no OBSs were deployed between 0- and 60-km model distance and (ii) no clear PmP arrivals were observed from OBSs s000 to s009 deployed in this basin. Overall, however, this comparison shows that the final  $P$ -velocity model obtained after the traveltime tomography is reliable and can be used for a detailed analysis of lateral variations in crustal velocity structure (Figures 4c to 4j).

## 5. Results

The final  $P$  wave velocity model images the geometry of the sedimentary, crustal, and uppermost mantle layers to a depth of ~25 km (Figure 4b). To characterize the crustal structure of the Tasman Basin and the northern Lord Howe Rise structural domains, one-dimensional (1-D) velocity-depth profiles below the sediments are extracted at 10-km intervals along the profile (Figures 4c to 4j).

### 5.1. The Tasman Basin

In the Tasman Basin, the sedimentary thickness is relatively constant and averages 2 km (Figure 4b). The velocity of the sediments ranges from 2.0 to 2.8 km/s. The underlying crust is ~6.5 km thick with velocities ranging from 5.9 to 7.0 km/s (Figure 4c). The Moho lies at a depth of 14 km below sea level, and the uppermost mantle is characterized by velocities of 7.9 km/s. Comparison between 1-D velocity-depth profiles of the crust and upper mantle in the Tasman Basin with those of the Atlantic Ocean (White et al., 1992) shows a consistent trend between the two, which confirms the oceanic nature of the basin's crust (Figure 4c).

East of the Tasman Basin, the crustal thickness increases progressively from 8 to 13 km (Figure 4d) over a 40-km-wide necking zone (from 95- to 135-km model distance). At 120-km model distance, a 1.7-km high seafloor escarpment marks the sharp boundary between the Tasman Basin and the Dampier Ridge.

### 5.2. The Dampier Ridge

At the Dampier Ridge (135- to 245-km model distance), we image some sedimentary basins with depocenter thicknesses that increase toward the eastern edge of the ridge up to a maximum thickness of ~4 km (Figure 4b). The velocity within the sediments ranges from 2.0 to 3.5 km/s, except in the basin located between 180- and 210-km model distance where the velocity in the sediments reaches 5.1 km/s (Figure 4b). The  $P$  wave velocity at the top of the crust ranges from 5.3 to 6.0 km/s (continuous orange lines in Figure 4e). The lowest upper crustal velocities (5.0 km/s) on the Dampier Ridge are modeled on a basement high at 220-km model distance (dashed orange line in Figure 4e). Basement highs on the Dampier Ridge have previously been interpreted as Miocene volcanic intrusions (Willcox et al., 2001), which is inconsistent with the modeled velocities. At the base of the crust, the velocity is homogenous with a characteristic value of 7.1 km/s. The transition to the uppermost mantle is characterized by a velocity step to 8 km/s at the top of the mantle. This is recorded by strong reflected arrivals from the Moho on the OBSs (Figures 2c and 2d). This suggests that no serpentized mantle exists at depth below the Dampier Ridge. The presence of igneous intrusions in the lower crust of the Dampier Ridge cannot be excluded in the depth range 13–18 km below sea level where velocities range between 6.8 and 7.1 km/s, but velocity-depth trends do not show a change of velocity gradient in the lower crust (Figure 4e).

The thickness of the crust under the Dampier Ridge ranges between 14 and 18 km (Figure 4e). This is within the range of crustal thicknesses modeled on the NE Atlantic passive margin where fragments of thinned continental crust have been described (Funck et al., 2016). At the Jan Mayen Ridge in the North Atlantic and the Sao-Paulo Plateau Ridge in the South Atlantic, the velocity of the crust ranges from 5.2 to 6.9 km/s, with a low-velocity gradient (Klingelhofer et al., 2014; Kodaira et al., 1998). The velocities in these regions are similar to those of the Dampier Ridge. Thus, we confirm the continental nature of the Dampier Ridge.

### 5.3. The Middleton Basin and Its Flanks

From the Dampier Ridge toward the Middleton Basin, the crust progressively thins over a 70-km-wide necking zone from 245- to 315-km model distance (Figure 4f). In this domain, the crust is composed of two layers. The upper crust is 3 km thick, and the lower crust is 6 to 9 km thick. The 1-D velocity-depth profiles are characteristic of a thinned continental crust with low gradients in the two crustal layers (Christensen & Mooney, 1995). The Moho is marked by a strong velocity contrast between the base of the crust and the upper mantle, suggesting the absence of mantle exhumation below the necking domain. The velocity of the uppermost mantle is 8.0 km/s.

The Middleton Basin is the deepest and widest basin along the profile (Figure 4b). The sediment infill is ~3.5 km thick, with velocity ranging from 1.8 to 3.7 km/s. Below, the 7-km-thick crust is very homogenous and is characterized by an upper crust that is 2 km thick with velocity ranging from 5.75 to 6.5 km/s and a 5-km-thick lower crust with velocities of 6.5 to 7.0 km/s (Figure 4g). The Moho is flat below the Middleton Basin and lies at a depth of 14 km below sea level (Figure 4b). The uppermost mantle is characterized by

velocities of 7.9 km/s. The 1-D velocity-depth profiles under the Middleton Basin correspond with those of oceanic crust in the Atlantic Ocean (Figure 4g).

The transition between the Middleton Basin and the Lord Howe Rise corresponds to a narrow (50-km wide) region where the crust progressively thickens to 22 km from 405- to 465-km model distance (Figure 4b). The crust has two layers, with an upper crustal layer characterized by a steep velocity gradient and a lower crustal layer characterized by a gentle velocity gradient (Figure 4h). In this necking zone, the upper crustal velocities are characterized by very low values of 4.25 km/s. These low velocities in the upper crust may be the result of faulting of the crust during extension and thinning. The Moho is a sharp boundary, and within this necking domain, seismic velocities in the lower crust of 6.5–7.0 km/s do not support the presence of magmatic underplating that would have velocities of 7.1–7.4 km/s (e.g., Hopper et al., 2003). Seismic velocities immediately below the Moho of this necking zone are typical of the uppermost mantle.

#### 5.4. The Western and Central Rift Provinces of the Lord Howe Rise

Crustal structure below the Western and Central Rift Provinces of the Lord Howe Rise does not vary greatly (Figure 4b). However, some characteristics of the crustal velocities allow distinctions to be made (Figure 4i and 4j). In the Western Rift Province (465- to 565-km model distance), the thickness of the sediments reaches 4 km in the main depocenters and their characteristic velocities are 1.6–3.3 km/s (Figure 4b). Below the depocenters the upper crustal velocities range from 5.6 to 6.4 km/s. At the base of the crust the velocity reaches 7.1 km/s (Figure 4i). On average, the crust under the Western Rift Province is 18 km thick (Figure 4i), but the Moho shows a subtle shallowing at 500-km model distance (Figure 4b).

Further to the east in the Central Rift Province (565- to 682-km model distance), the thickness of the sediments is less than in the Western Rift Province (Figure 4b), with an average thickness of 1.5 km. The velocities in the sediments range from 1.8 to 2.7 km/s (Figure 4b). At the top of basement, velocities range from 4.9 to 6.1 km/s and increase with depth to reach 7.0 km/s at the bottom of the crust. Below the Central Rift Province, the crust is ~22 km thick (Figure 4j) and the Moho is relatively flat.

Comparison of Lord Howe Rise 1-D velocity-depth profiles to those from typical continental crust (Christensen & Mooney, 1995) shows strong similarities (Figures 4i and 4j). Therefore, we confirm the continental nature of the Lord Howe Rise. Our results also highlight an increase in the thinning of the crust from the Central Rift Province toward the Middleton Basin.

## 6. Discussion

### 6.1. Nature of the Crust Below the Middleton Basin

The existence of thin crust below the Middleton Basin was previously reported based on a seismic experiment using an expanding spread profile acquired across the basin (Figure 1b; Shor et al., 1976). The interpretation of this profile showed that the depth of the Moho increases from 13 km in the center of the basin to 17.5 km close to the Dampier Ridge, with an associated crustal thickness of 5 to 12 km, respectively (Shor et al., 1976). Understanding the nature of the crust that floors this basin is a crucial constraint on the rifting history of the eastern Gondwana margin. However, none of the previous geophysical data acquired across the basin has allowed any inferences on the nature of the crust and upper mantle beneath the Middleton Basin.

We can first look at how our results compare to the end-member archetypes of magma-poor or magma-rich rifted margins (e.g., Franke, 2013; Mutter et al., 1988; Reston, 2009; White et al., 1987). Wide-angle seismic data at magma-rich rifted margins typically show *P* wave velocity in the lower crust of 7.1–7.4 km/s (e.g., Fromm et al., 2015; Hopper et al., 2003). The general lack of high-velocity lower crust and the absence of changes in lower crustal velocity gradients (Figures 4 and S3) leads to the interpretation that northwestern Zealandia is a magma-poor margin. It is important to note that volcanism is found throughout this region before and after breakup (e.g., Bryan et al., 1997; Mortimer et al., 2018; Tulloch et al., 2009), potentially indicating timing variations for tectono-magmatic interactions and melt production for the margin.

The interpretation that this is a magma-poor margin suggests three potential lithologies for the crust below the Middleton Basin. Based on wide-angle seismic profiles acquired across passive margins in other parts of the world, different interpretations have been made regarding the nature of the crust and upper mantle

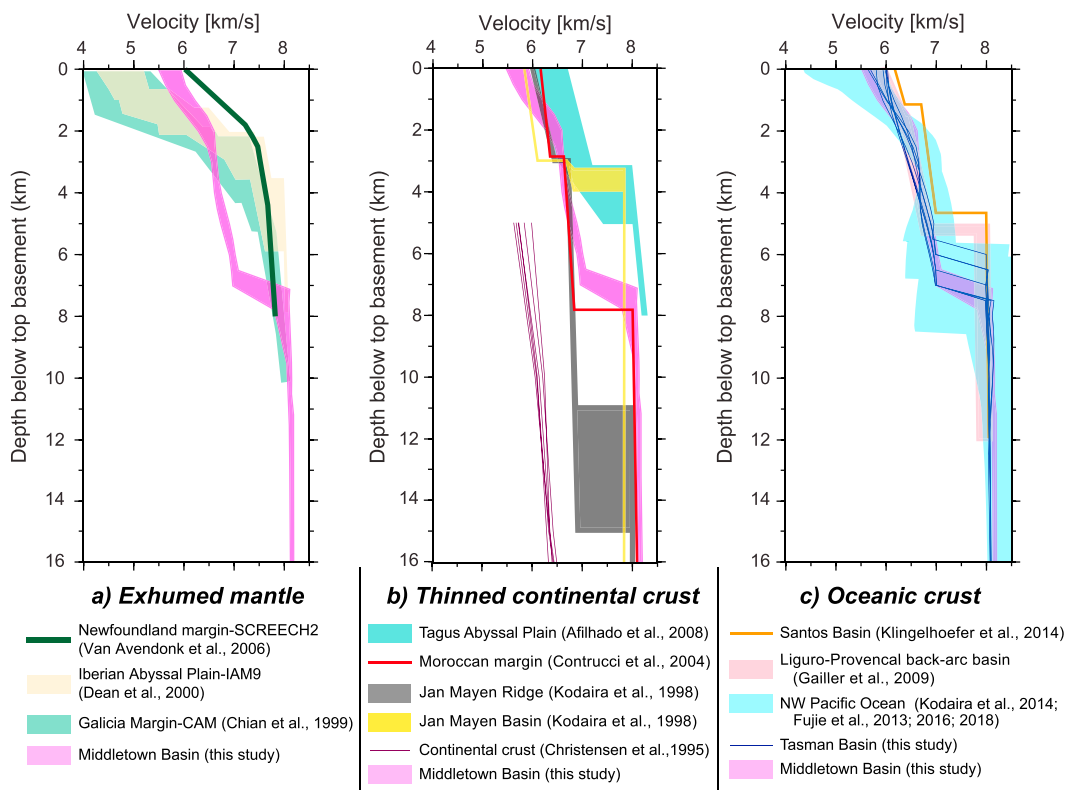


**Figure 6.** 1-D velocity-depth profiles below top basement extracted in the Middleton Basin and, for comparison, 1-D velocity-depth profiles that are characteristic of various crustal types. (a) Exhumed mantle/serpentinized peridotites: The Galicia margin (Chian et al., 1999), the Iberian margin (Dean et al., 2000), and the Newfoundland margin (van Avendonk et al., 2006). (b) Thinned continental crust: typical continental crust (Christensen & Mooney, 1995), the Jan Mayen ridge and basin (Kodaira et al., 1998), the Moroccan margin (Contrucci et al., 2004), and the Tagus abyssal plain (Afilhado et al., 2008). (c) Oceanic crust: The Tasman Basin (this study), the NW Pacific Ocean >100 km from the Japan trench (Fujie et al., 2013, 2016, 2018; Kodaira et al., 2014), the Liguro-Provencal Basin (Gailler et al., 2009), and the Brazilian margin in the Santos Basin (Klingelhoefer et al., 2014).

in the continent-ocean transition zone of magma-poor margins: (i) exhumed mantle emplaced during the last stage of rifting (Chian et al., 1999; Dean et al., 2000; van Avendonk et al., 2006; Whitmarsh et al., 2001), (ii) highly thinned continental crust with extreme stretching during rifting of the margin (Klingelhöfer et al., 2005; Kodaira et al., 1998), and (iii) oceanic crust formed during the early stages of oceanic accretion (Gailler et al., 2009; Klingelhoefer et al., 2014). The Middleton Basin lies between two known continental fragments, the Dampier Ridge and the Lord Howe Rise, and is therefore ideally suited to distinguishing these three possibilities for the nature of the crust and upper mantle below continent-ocean transition zones on magma-poor margins. To aid in making this distinction for the Middleton Basin, we compiled 1-D velocity-depth profiles below the top of basement for comparison with published 1-D velocity-depth profiles of known crustal types.

### 6.1.1. Exhumed Mantle

The first hypothesis for the nature of the basement underlying the Middleton Basin is that it is exhumed continental mantle. Since the drilling of serpentinized upper mantle rocks at the continent-ocean transition of the Iberia margin (Whitmarsh et al., 2001), several wide-angle studies of nonvolcanic passive margins have inferred the existence of exhumed mantle in the transitional domain (Chian et al., 1999; Dean et al., 2000; van Avendonk et al., 2006). Numerical modeling has confirmed that exhumation can take place during the last phase of rifting (Lavier & Manatschal, 2006). The  $P$  velocity of the exhumed mantle is characterized by an upper 2- to 3-km-thick layer with a high-velocity gradient overlying a lower layer where the velocities progressively increase with depth (Figure 6a; Chian et al., 1999; Dean et al., 2000; van Avendonk et al., 2006). Comparison between the 1-D velocity-depth profiles from the Middleton Basin and those from areas of inferred exhumed mantle shows that the upper layer of the crust in the Middleton Basin has a lower

velocity gradient (Figure 6a). Unlike places where exhumed mantle has been inferred, we also observe a strong reflection at the Moho in both the MCS and the OBS data. This strong reflection coincides with a strong velocity step between the base of the crust and the uppermost mantle (Figures 2e to 2h and 4a). Therefore, we rule out the presence of exhumed mantle beneath the Middleton Basin.

### 6.1.2. Highly Thinned Continental Crust

Based on wide-angle seismic studies, it has been shown that the thinning of the continental crust at passive margins can be extreme. Very thin continental crust (<5 km) has been modeled at the Jan Mayen Basin in the North Atlantic margin and at the Tagus Abyssal Plain in the Iberian margin (Figure 6b; Afilhado et al., 2008; Kodaira et al., 1998). In this context, the 7-km-thick crust of the Middleton Basin could still be of continental origin.

The thinned continental crust imaged at passive margins from around the world is characterized by a two layered crustal structure with a low-velocity gradient in the upper and lower crusts (Figure 6b; Afilhado et al., 2008; Contrucci et al., 2004; Kodaira et al., 1998). We found a high-velocity gradient in the upper crustal layer beneath the Middleton Basin that does not match the characteristic gradient of highly-thinned continental crust (Figure 6b). The upper crustal velocity of thinned continental crust is generally higher than 5.9 km/s (Afilhado et al., 2008; Contrucci et al., 2004; Kodaira et al., 1998). In the Middleton Basin, the range of upper crustal velocity is slightly slower than typical thinned continental crust (5.5 to 6.0 km/s).

Extreme stretching and thinning of continental crust are associated with normal faults that bound blocks of upper-middle crust and rifted basins (Lavier & Manatschal, 2006). If the Middleton Basin is floored by continental crust, these features might have been preserved in the crust. Crustal fault blocks are not evident below the Middleton Basin (Figure 4a), where the top of the basement is instead flat, reflecting little deformation. It seems unlikely that the stretching of the continental crust could create such a homogenous crust with a clear Moho reflection recorded by both the MCS and the OBS data in the Middleton Basin (Figures 2e to 2h). Additionally, some studies of North Atlantic margins have shown that the upper mantle beneath thinned continental crust can be serpentinized (e.g., Pérez-Gussinyé & Reston, 2001), likely due to basement faults controlling hydration of the upper mantle (Bayrakci et al., 2016). In the Middleton Basin, the lack of basement structures and seismic-velocity evidence for serpentinized mantle suggests a different formation process. Based on the observations of the seismic velocity and multichannel seismic, we conclude that the Middleton Basin is not likely to be floored by thinned continental crust.

### 6.1.3. Oceanic Crust

The last hypothesis for the nature of the crust of the Middleton Basin is an oceanic crust that formed following separation of the Dampier Ridge from the Lord Howe Rise (Gaina, Müller, et al., 1998; Gaina, Roest, et al., 1998). In the multichannel seismic data, the crust of the Middleton Basin displays some characteristics of oceanic crust. The crust has a thickness of ~2-s twt and a Moho reflection imaged at 9.5-s twt (Figure 4a; Boston et al., 2019).

In the Atlantic Ocean, the oceanic crust is  $7.1 \pm 0.8$  km thick and corresponds to a two-layered crust characterized by a high-velocity gradient in the upper crust and gentle gradient in the lower crust (White et al., 1992). Comparison between the structure of the crust beneath the Middleton Basin and the Atlantic Ocean and northwest Pacific Ocean crust shows a similar thickness and similar velocity gradients in the upper and lower crust (Figures 4g and 6c). However, higher velocities are modeled at the top of the crust of the Middleton Basin (5.5 to 6.0 km/s) compared to those of the Atlantic Ocean (4.0 to 5.5 km/s; Figure 4g), but within the range of velocities for the northwest Pacific Ocean (4.4 to 6.0 km/s; Figure 6c). The narrow width of the Middleton Basin (<120 km) suggests that if the crust of the basin is oceanic, the structure of the crust might record the early stage of spreading to form a new ocean with a velocity structure that is closer to the northwest Pacific Ocean than the Atlantic Ocean.

Few geophysical studies have focused on the oceanic crust accreted during the initial stages of oceanic spreading, but some examples are documented in the Liguro-Provencal Basin in the Mediterranean Sea (Gailler et al., 2009) and on the Brazilian margin (Evain et al., 2015; Klingelhoefer et al., 2014). On these margins, the initial oceanic crust is 5 km thick and is characterized by relatively high velocity on top of the crust (Figure 6c; Gailler et al., 2009; Klingelhoefer et al., 2014). Comparison between the crust imaged at those margins and the crust of the Middleton Basin reveals an almost perfect similarity between the 1-D velocity-depth profiles (Figure 6c). This is a strong indication that the crust of the Middleton Basin is

oceanic. Finally, our seismic transect also crossed the Tasman Basin, one of the few well-constrained basins in this region that is unequivocally oceanic in nature. Our tomographic analysis reveals that both the crustal thickness and the velocity-depth trend below the Middleton Basin and the Tasman Basin are similar. Due to the proximity of these basins and the fact that both have been modeled using the same technique, we suggest that these similarities are a further indication that the crust of the Middleton Basin is oceanic.

## 6.2. Rifting of Northern Zealandia

Combining our results (Figure 4b) with previous wide-angle seismic studies (Klingelhoefer et al., 2007), an expanding spread profile (Shor et al., 1976), and passive seismic crustal constraints (Clitheroe et al., 2000; Sun & Kennett, 2016) provides regional crustal constraints across the breakup of eastern Gondwana (Figure 7). Previous MCS data suggest a much sharper (~50 km) boundary for eastern Australia (van de Beuque et al., 2003) than seen in passive seismic data (Clitheroe et al., 2000; Sun & Kennett, 2016), but both of these data sets show a much narrower eastern Australian margin compared to the conjugate margin of northern Zealandia that extends over a width of >1,000 km from the Dampier Ridge to the Norfolk Ridge. Thus, the breakup of eastern Gondwana was highly asymmetric.

The Lord Howe Rise shows a fairly constant crustal thickness of 20–23 km and consistent 1-D velocity trends across survey locations (Figure 7c). This indicates similar thinning and rifting processes across this ~400-km-wide continental fragment that may have later influenced how it submerged. Other wide margins such as the South China Sea exhibit less uniform thinning at similar distances from the continent-ocean transitions (Pichot et al., 2014). Previous work suggests that higher than normal heat flow is needed to create a wide margin (Buck et al., 1999), which in Zealandia could be related to the formation of Whitsunday Volcanic Province that was active during the Early Cretaceous prior to the onset of extension across northern Zealandia (Bryan et al., 1997), or to the presence of a *diffuse alkaline magmatic province* in the southwest Pacific that is unrelated to a plume or specifically to rifting (Finn et al., 2005; Mortimer et al., 2018).

In the Western Rift Province, the Moho of the Lord Howe Rise shows a subtle shallowing at 1,175-km model distance (Figure 7b). We suggest that this gentle Moho relief is most likely related to the deeper basins and greater extension on the western side of the Lord Howe Rise. However, the Lord Howe Rise is known to be latitudinally segmented by the NE-SW oriented Barcoo-Elizabeth-Fairway Lineament, a crustal-scale feature with a gravity and seismic expression (Figure 1b; Stagg et al., 1999; Willcox et al., 2001). This lineament may have also influenced crustal structure.

The Dampier Ridge is one of the thinnest (14–18 km) regions of continental crust with more typical continental velocity profiles. It is bounded on both sides by thinner crust (Figure 4) and is similar to the Fairway Ridge and Norfolk Ridge further to the east where thin continental crust is also bound by thinner crust (Figure 7b). These parts of Zealandia have 1-D velocity trends that are similar to other proposed thin continental ridges such as the Jan Mayen Ridge and the Rockall Trough (Figure 7d). Furthermore, thin crust is found well inboard of the continent-ocean transition at other wide margins such as the South China Sea (Pichot et al., 2014; Qiu et al., 2001), which may be a characteristic indication of the processes that form wide margins.

There are three regions of very thin crust within northern Zealandia: the Middleton Basin, the Fairway Basin, and the New Caledonia Trough. Comparison of these regions shows that the Middleton Basin contains the thinnest crust (Figure 7e), and the inferred existence of oceanic spreading in the Middleton Basin places an earlier stage of breakup ~300 km to the east of the main breakup that formed the Tasman Basin. Whereas the Fairway Basin is thought to be underlain by continental crust thinned to 12–15 km, velocity trends in the New Caledonia Trough indicate both continental and oceanic patterns depending on the profile location (Klingelhoefer et al., 2007). MCS data also show that parts of the New Caledonia Trough are underlain by deep rifted basins (Sutherland et al., 2010), but other parts are characterized by largely undeformed basement (Collot et al., 2009). Eocene initiation of Tonga-Kermadec subduction may have caused the rapid Cenozoic subsidence and sedimentation evident in the New Caledonia Trough (Sutherland et al., 2010), but basement lithology and structure would still be related to earlier rifting events and therefore provide evidence for the way in which the crust of this wide margin deformed before final breakup in the Tasman Basin.

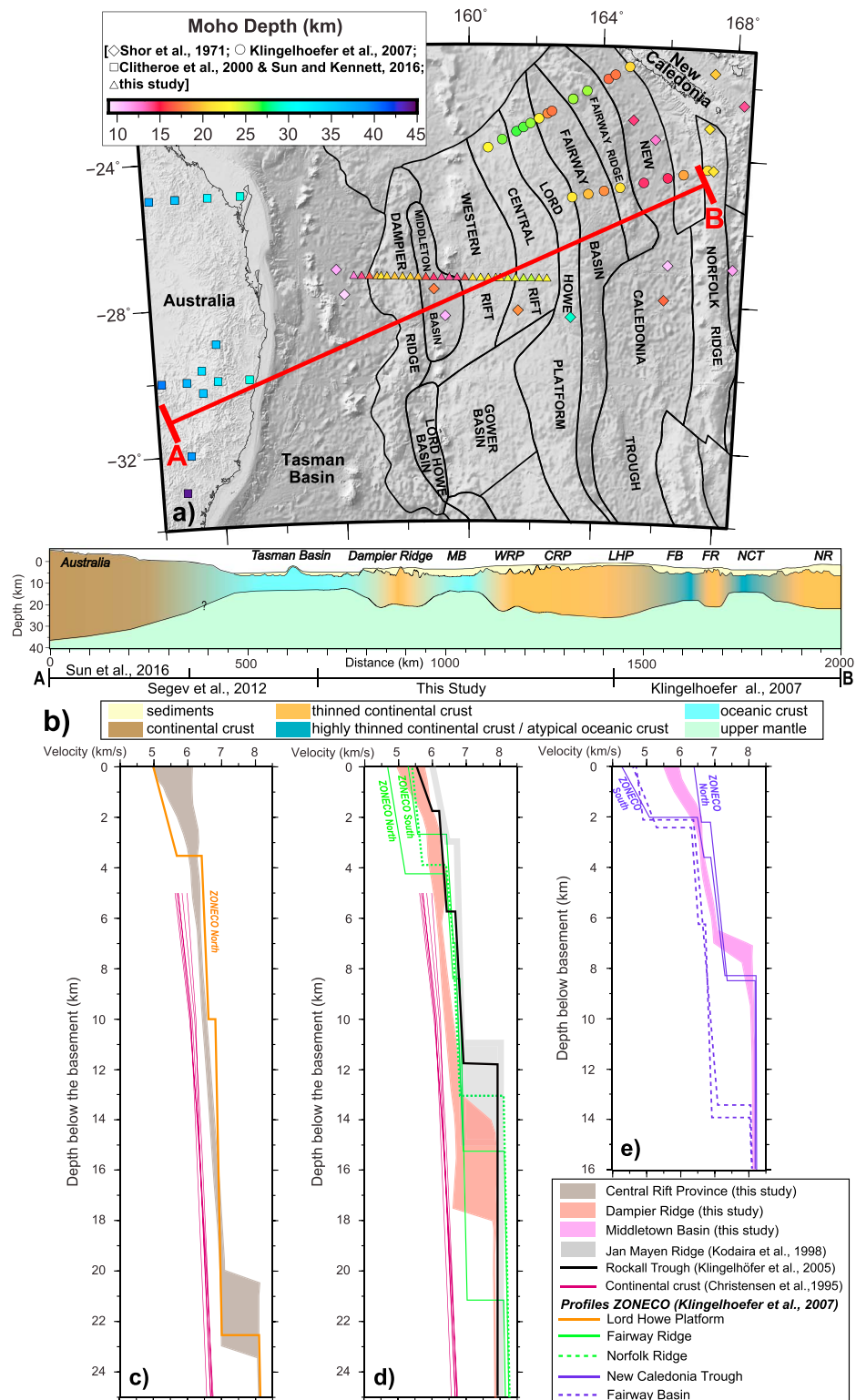


**Figure 7.** Regional profile illustrating crustal structure across northern Zealandia. (a) Shaded relief map with Moho depth constraints from this study and previous studies. The red line shows the location of Figure 7b. (b) Projected cross section across northern Zealandia with Moho depths and interpreted crustal lithology. MB, Middleton Basin; WRP, Western rift Providence; CRP, central rift Providence; FB, Fairway Basin; FR, fairway ridge; NCT, New Caledonia trough; NR, Norfolk ridge. 1-D velocity-depth profiles for northern Zealandia in comparison to profiles from other areas: (c) continental crust, (d) ridges, and (e) basins.

### 6.3. Plate Kinematic and Geodynamic Implications

The crustal geometry across the north Tasman Basin and the northern Lord Howe Rise, together with the new evidence for oceanic crust beneath the Middleton Basin, allows a review of the proposed geodynamic evolution of the eastern Gondwana margin. An early model to explain the asymmetry between the conjugate eastern Australian and northern Zealandia margins (comprising the Dampier Ridge-Middleton Basin-Lord Howe Rise-New Caledonia Trough-Norfolk Ridge; Figure 1) invoked crustal-scale detachments (Lister et al., 1991). In this model, eastern Australia is interpreted as an upper plate margin and northern Zealandia as the corresponding lower plate margin that is underlain by an undulating detachment that shallows beneath the Middleton Basin and the New Caledonia Trough. This undulating detachment resulted in a smooth top of basement for those regions (Lister et al., 1991). However, our results suggest that oceanic crust floors the Middleton Basin, and the central New Caledonia Trough has previously been inferred to be floored by oceanic crust, at least in part (Klingelhoefer et al., 2007). These observations are not consistent with the presence of an undulating detachment in continental crust beneath the Middleton Basin or the New Caledonia Trough. In addition, the narrow and relatively symmetrical continent-ocean transitions on either side of the Middleton Basin (Figure 4) are more consistent with a classical pure-shear extensional model rather than a simple shear model incorporating a crustal-scale detachment.

Kinematic reconstructions have shown that the Middleton Basin and its southward extension, the Lord Howe Basin, opened during pre-Tasman rifting between the Dampier Ridge and the northern Lord Howe Rise (Gaina, Müller, et al., 1998; Gaina, Roest, et al., 1998; Jongsma & Mutter, 1978). The absence of linear magnetic anomalies in the Middleton Basin linked to seafloor spreading led Gaina, Müller, et al. (1998); Gaina, Roest, et al. (1998) to exclude the possibility of finding oceanic crust below this basin. However, our seismic velocity model now provides evidence for oceanic crust under the Middleton Basin. The absence of clear magnetic anomalies in this oceanic basin could be explained by the thick sedimentary cover or Miocene volcanic activity associated with the Lord Howe hot spot trail, which might have masked the oceanic spreading fabric. An explanation similar to the second possibility has already been proposed for the north Tasman Basin where linear magnetic anomalies linked to seafloor spreading are also very sparse (Gaina, Müller, et al., 1998; Gaina, Roest, et al., 1998). When combined with the previous opening models for this region (Jongsma & Mutter, 1978), our results imply that the Lord Howe Basin is also floored by oceanic crust. We therefore propose that rifting between the Dampier Ridge and the northern Lord Howe Rise led to the formation of oceanic crust in the Middleton and Lord Howe Basins in the Late Cretaceous, just before the opening of the northern Tasman Basin. If these ~100-km-wide basins formed from 84 to 72 Ma, then the half spreading rate is <1 cm/year. While this is a very slow spreading rate, it is comparable to the <2 cm/year half spreading rate of the Tasman Basin (Müller et al., 2008).

Plume-driven processes have previously been invoked to explain the formation of various features found within and adjacent to northern Zealandia. For example, it has been proposed that a thermal anomaly (e.g., a plume) can cause an active oceanic ridge to jump to the landward edge of a young continental margin with the subsequent formation of a microcontinent (Gaina et al., 2003; Mittelstaedt et al., 2008; Müller et al., 2001). The presence of two distinct thermal anomalies under the central Lord Howe Rise and the Ross Sea has been used to explain two jumps by the south Tasman Basin spreading ridge that led to the isolation of the East Tasman Plateau and the Gilbert Seamount microcontinents (Gaina et al., 2003; Müller et al., 2001). Based on the new finding of oceanic crust below the Middleton Basin and on the presence of late Cretaceous-early Cenozoic plume-related volcanism in eastern Australia (Sutherland & Fanning, 2001), it is possible that the cessation of seafloor spreading in the Lord Howe/Middleton Basins and the isolation of the Dampier Ridge could be the result of a plume-related jump leading to microcontinent formation.

A problem with invoking plume-driven processes as a driver for eastern Gondwana fragmentation is the lack of evidence for high-velocity underplating or igneous intrusion in the lower crust of our crustal seismic velocity model (Figure 4), which suggests that northwestern Zealandia is a magma-poor margin. This is consistent with the volcanotectonic regime of this region discussed by Mortimer et al. (2018), who show that other than the time-progressive Oligocene-Recent Lord Howe and Tasmantid seamount chains, low volume and widely scattered Late Cretaceous to Holocene volcanism in this region is not related to plumes but could instead be derived from diffuse asthenospheric or lithospheric sources.

Given the lack of evidence in crustal seismic velocities for voluminous magmatic activity associated with plume-driven extension and breakup, the formation of northern Zealandia could instead be linked to rollback of a subducting slab at the eastern Gondwana margin (Schellart et al., 2006). Rey and Müller (2010) show that if subduction velocity decreases, stresses induced by the buoyant mantle wedge above a subducting slab can drive trench retreat. This trench retreat can lead to gravitational collapse of an Andean-type cordillera mountain range at the convergent margin and ultimately the detachment of microcontinents and breakup of the active plate margin. In the case of the eastern Gondwana margin, subduction velocity probably decreased at around 105–90 Ma as the Australian continent began to move northward away from Antarctica (Rey & Müller, 2010). Göğüş (2015) has also shown that the combination of slab rollback and removal of upper-plate lithospheric (via delamination or convective removal) can trigger and facilitate the development of broad extension in continental back arcs. This model also requires the collapse of thickened orogenic lithosphere and linked postorogenic lithospheric removal.

A metamorphic core complex in New Zealand has been interpreted as evidence for a collapsed cordillera at the eastern Gondwana margin (Tulloch & Kimbrough, 1989), but there is currently no clear evidence for a cordillera mountain range in the Lord Howe Rise region. In fact, with no clear expression of volcanic chains, accretionary wedges or paleo trenches in bathymetry or seismic data, there is currently no compelling evidence for the presence of Late Cretaceous to Paleocene subduction under northern Zealandia (Mortimer et al., 2018). This inference is consistent with the petrology and geochemistry of high-volume magmatic activity associated with an extensive silicic large igneous province that was active during the Early Cretaceous along the entire length of eastern Australia, probably much of the Lord Howe Rise and into New Zealand (Bryan et al., 1997). This volcanic activity has been invoked as the trigger for eastern Gondwana breakup (Bryan et al., 1997; Tulloch et al., 2009), but the petrology and geochemistry of these lavas indicates volcanism linked to intracontinental rifting not back-arc extension. The most recent synthesis of geochemical data from altered samples dredged from northern Zealandia also suggests that lavas in this region predominantly have an intraplate signature that reflects continental rifting processes rather than subduction (Mortimer et al., 2018).

Finally, Molnar et al. (2018) describe analogue models that show microcontinents can form at continental margins characterized by rotational extensional kinematics in the presence of a linear, lithospheric-scale weakness at a low-angle to the rift axis. These models were used to explain the formation of relatively small microcontinents like the East Tasman Plateau and the Gilbert Seamount in the Tasman Sea, the Flemish Cap and the Galicia Bank in the Atlantic, or the Danakil Block in the Red Sea, and they may also explain the separation of the Dampier Ridge from the Lord Howe Rise in response to the oceanic spreading inferred in the Middleton and Lord Howe Basins. The possible existence of a lithospheric weakness in the Tasman Sea remains to be determined.

## 7. Conclusions

Tomographic modeling of wide-angle seismic data across northern Zealandia has been used to delineate several distinct crustal domains:

1. The northern Tasman Basin that is floored by 7-km thick oceanic crust.
2. The Dampier Ridge and the western side of the Lord Howe Rise that represent two extended and thinned continental fragments with a crustal thickness of ~16 and ~20 km, respectively.
3. The Middleton Basin, between the two continental fragments, that has ~3.5 km of sediment overlying ~7-km-thick crust. The velocity gradient of the two-layered crust beneath the Middleton Basin is characteristic of oceanic crust.
4. Necking zones between the oceanic Middleton Basin and the adjacent extended continental fragments are narrow (<70 km), relatively symmetric (i.e., indicative of classical pure shear), and there is no clear evidence for mantle exhumation or intrusion/underplating of high-velocity material.

We suggest therefore that the northwestern margin of Zealandia is magma-poor and lacks evidence for hyperextension. The absence of evidence for magmatism in the deeper crust presents problems for plume-driven models of rifting and breakup at the eastern Gondwana margin. Instead, processes linked to eastward rollback of west dipping subduction beneath the eastern Gondwana margin throughout the Cretaceous and into the Cenozoic may be more appropriate. However, evidence for a subduction-related magmatic arc on or

adjacent to the Lord Howe Rise remains elusive, as is unequivocal evidence for a cordillera mountain range that collapsed in response to the retreat of the subducting slab.

While the results of this study provide a better understanding of the crustal structure of the enigmatic northern Zealandia continental fragment, many uncertainties around the processes that drove the breakup of eastern Gondwana remain. Further understanding of this enigmatic margin awaits integration with regional stratigraphic interpretations that also require more rigid constraints on the lithology and age of basin-fill sediments and underlying basement of the Dampier Ridge, Middleton Basin and Lord Howe Rise.

### Acknowledgments

The authors wish to thank the captain, officers, crew, and technical staff of the R/V *Kairei* for support during data acquisition during the KR16-05/GA0354 survey (the cruise report can be downloaded at: [http://www.godac.jamstec.go.jp/catalog/doc\\_catalog/metadataDisp/KR16-05\\_leg1-3\\_all](http://www.godac.jamstec.go.jp/catalog/doc_catalog/metadataDisp/KR16-05_leg1-3_all)). This work was funded and conducted under a Collaborative Head Agreement between the Japan Agency for Marine-Earth Science and Technology and Geoscience Australia that includes planning for deep riser drilling on the Lord Howe Rise under the International Ocean Discovery Program (Proposal 871-CPP). The GMT graphics package was used to create the maps and figures (Wessel & Smith, 1998). We thank T. Shirai, T. Sato, and B. Marcaillou for their help and fruitful discussions during this study. We also thank Alexey Goncharov, Merrie-Ellen Gunning, Harm van Avendonk, and Julien Collot for their constructive and detailed reviews, which greatly improved the manuscript. Ron Hackney publishes with the permission of the Chief Executive Officer, Geoscience Australia. All the seismic survey data can be requested from JAMSTEC crustal structural database site ([https://www.jamstec.go.jp/jamstec-e/IFREE\\_center/index-e.html](https://www.jamstec.go.jp/jamstec-e/IFREE_center/index-e.html)).

### References

- Afilhado, A., Matias, L., Shiobara, H., Hirn, A., Mendes-Victor, L., & Shimamura, H. (2008). From unthinned continent to ocean: The deep structure of the West Iberia passive continental margin at 38°N. *Tectonophysics*, 458(1–4), 9–50. <https://doi.org/10.1016/j.tecto.2008.03.002>
- Aslanian, D., Moulin, M., Olivet, J.-L., Unternehr, P., Matias, L., Bache, F., et al. (2009). Brazilian and African passive margins of the Central Segment of the South Atlantic Ocean: Kinematic constraints. *Tectonophysics*, 468(1–4), 98–112. <https://doi.org/10.1016/j.tecto.2008.12.016>
- van Avendonk, H. J. A., Holbrook, W. S., Nunes, G. T., Shillington, D. J., Tucholke, B. E., Louden, K. E., et al. (2006). Seismic velocity structure of the rifted margin of the eastern Grand Banks of Newfoundland, Canada. *Journal of Geophysical Research*, 111, B11404. <https://doi.org/10.1029/2005JB004156>
- Bayrakci, G., Minshull, T. A., Sawyer, D. S., Reston, T. J., Klaeschen, D., Papenberg, C., et al. (2016). Fault-controlled hydration of the upper mantle during continental rifting. *Nature Geoscience*, 9(5), 384–388. <https://doi.org/10.1038/ngeo2671>
- Boston, B., Nakamura, Y., Gallais, F., Gou, F., Kodaira, S., Miura, S., et al. (2019). Delayed subsidence after rifting and a record of breakup for northwestern Zealandia. *Journal of Geophysical Research: Solid Earth*, 124. <https://doi.org/10.1029/2018JB016799>
- Bryan, S. E., Constantine, A. E., Stephens, C. J., Ewart, A., Schön, R. W., & Parianos, J. (1997). Early Cretaceous volcano-sedimentary successions along the eastern Australian continental margin: Implications for the break-up of eastern Gondwana. *Earth and Planetary Science Letters*, 153(1–2), 85–102. [https://doi.org/10.1016/S0012-821X\(97\)00124-6](https://doi.org/10.1016/S0012-821X(97)00124-6)
- Buck, W. R., Lavier, L. L., & Poliakov, A. N. B. (1999). How to make a rift wide. *Philosophical Transactions of the Royal Society A: Mathematical, Physical and Engineering Sciences*, 357(1753), 671–693. <https://doi.org/10.1098/rsta.1999.0348>
- Chian, D., Louden, K. E., Minshull, T. A., & Whitmarsh, R. B. (1999). Deep structure of the ocean-continent transition in the southern Iberia Abyssal Plain from seismic refraction profiles: Ocean Drilling Program (Legs 149 and 173) transect. *Journal of Geophysical Research*, 104(B4), 7443–7462. <https://doi.org/10.1029/1999JB900004>
- Christensen, N. I., & Mooney, W. D. (1995). Seismic velocity structure and composition of the continental crust: A global view. *Journal of Geophysical Research*, 100(B6), 9761–9788. <https://doi.org/10.1029/95JB00259>
- Clitheroe, G., Gudmudsson, O., & Kennett, B. L. N. (2000). The crustal thickness of Australia. *Journal of Geophysical Research*, 105(B6), 13,697–13,713. <https://doi.org/10.1029/1999JB900317>
- Collot, J., Herzer, R., Lafoy, Y., & Géli, L. (2009). Mesozoic history of the fairway-aotea basin: Implications for the early stages of gondwana fragmentation. *Geochemistry, Geophysics, Geosystems*, 10, Q12019. <https://doi.org/10.1029/2009GC002612>
- Collot, J., Vendé-Leclerc, M., Rouillard, P., Lafoy, Y., & Géli, L. (2012). Map helps unravel complexities of the southwestern Pacific Ocean. *Eos, Transactions American Geophysical Union*, 93(1), 1. <https://doi.org/10.1029/2012EO010001>
- Contrucci, I., Matias, L., Moulin, M., Géli, L., Klingelhoefer, F., Nouzé, H., et al. (2004). Deep structure of the West African continental margin (Congo, Zaïre, Angola), between 5°S and 8°S, from reflection/refraction seismics and gravity data. *Geophysical Journal International*, 158(2), 529–553. <https://doi.org/10.1111/j.1365-246X.2004.02303.x>
- Crawford, A. J., Meffre, S., & Symonds, A. (2002). 120 to 0 Ma tectonic evolution of the southwest Pacific and analogous geological evolution of the 600 to 220 Ma Tasman Fold Belt System. *Geological Society of Australia Special Publication*, 22, 377–397.
- Dadd, K. A., Locmelis, M., Higgins, K., & Hashimoto, T. (2011). Cenozoic volcanism of the Capel-Faust Basins, Lord Howe Rise, SW Pacific Ocean. *Deep Sea Research Part II: Topical Studies in Oceanography*, 58(7–8), 922–932. <https://doi.org/10.1016/j.dsr2.2010.10.048>
- Dean, S. M., Minshull, T. A., Whitmarsh, R. B., & Louden, K. E. (2000). Deep structure of the ocean-continent transition in the southern Iberia Abyssal Plain from seismic refraction profiles: The IAM-9 transect at 40°20'N. *Journal of Geophysical Research*, 105(B3), 5859–5885. <https://doi.org/10.1029/1999JB900301>
- Eddy, D. R., van Avendonk, H. J. A., Christeson, G. L., & Norton, I. O. (2018). Structure and origin of the rifted margin of the northern Gulf of Mexico. *Geosphere*, 14(4), 1804–1817. <https://doi.org/10.1130/GES01662.1>
- Evain, M., Afilhado, A., Rigoti, C., Loureiro, A., Alves, D., Klingelhoefer, F., et al. (2015). Deep structure of the Santos Basin-São Paulo Plateau System, SE Brazil: Santos Basin-São Paulo Plateau Structure. *Journal of Geophysical Research: Solid Earth*, 120, 5401–5431. <https://doi.org/10.1002/2014JB011561>
- Finn, C. A., Müller, R. D., & Panter, K. S. (2005). A Cenozoic diffuse alkaline magmatic province (DAMP) in the southwest Pacific without rift or plume origin. *Geochemistry, Geophysics, Geosystems*, 6, Q02005. <https://doi.org/10.1029/2004GC000723>
- Franke, D. (2013). Rifting, lithosphere breakup and volcanism: Comparison of magma-poor and volcanic rifted margins. *Marine and Petroleum Geology*, 43, 63–87. <https://doi.org/10.1016/j.marpetgeo.2012.11.003>
- Fromm, T., Planert, L., Jokat, W., Ryberg, T., Behrmann, J. H., Weber, M. H., & Haberland, C. (2015). South Atlantic opening: A plume-induced breakup? *Geology*, 43(10), 931–934. <https://doi.org/10.1130/G36936.1>
- Fujie, G., Ito, A., Kodaira, S., Takahashi, N., & Kaneda, Y. (2006). Confirming sharp bending of the Pacific plate in the northern Japan trench subduction zone by applying a traveltimes mapping method. *Physics of the Earth and Planetary Interiors*, 157(1–2), 72–85. <https://doi.org/10.1016/j.pepi.2006.03.013>
- Fujie, G., Kodaira, S., Kaiho, Y., Yamamoto, Y., Takahashi, T., Miura, S., & Yamada, T. (2018). Controlling factor of incoming plate hydration at the north-western Pacific margin. *Nature Communications*, 9(1), 3844. <https://doi.org/10.1038/s41467-018-06320-z>
- Fujie, G., Kodaira, S., Sato, T., & Takahashi, T. (2016). Along-trench variations in the seismic structure of the incoming Pacific plate at the outer rise of the northern Japan Trench. *Geophysical Research Letters*, 43, 666–673. <https://doi.org/10.1002/2015GL067363>

- Fujie, G., Kodaira, S., Yamashita, M., Sato, T., Takahashi, T., & Takahashi, N. (2013). Systematic changes in the incoming plate structure at the Kuril trench. *Geophysical Research Letters*, 40, 88–93. <https://doi.org/10.1029/2012GL054340>
- Funck, T., Geissler, W. H., Kimbell, G. S., Gradmann, S., Erlendsson, Ö., McDermott, K., & Petersen, U. K. (2016). Moho and basement depth in the NE Atlantic Ocean based on seismic refraction data and receiver functions. *Geological Society, London, Special Publications*, 447(1), 207–231. <https://doi.org/10.1144/SP447.1>
- Gailler, A., Klingelhoefer, F., Olivet, J.-L., & Aslanian, D. (2009). Crustal structure of a young margin pair: New results across the Liguro-Provencal Basin from wide-angle seismic tomography. *Earth and Planetary Science Letters*, 286(1–2), 333–345. <https://doi.org/10.1016/j.epsl.2009.07.001>
- Gaina, C., Müller, R. D., Brown, B. J., & Ishihara, T. (2003). Microcontinent formation around Australia. *Geological Society of America Special Publication*, 372, 405–416. <https://doi.org/10.1130/0-8137-2372-8.405>
- Gaina, C., Müller, R. D., Royer, J. Y., Stock, J., Hardebeck, J., & Symonds, P. A. (1998). The tectonic history of the Tasman Sea: A puzzle with 13 pieces. *Journal of Geophysical Research*, 103(B6), 12,413–12,433. <https://doi.org/10.1029/98JB00386>
- Gaina, C., Roest, W., Müller, R. D., & Symonds, P. A. (1998). The opening of the Tasman Sea: A gravity anomaly animation. *Earth Interactions*, 2(4), 1–23. [https://doi.org/10.1175/1087-3562\(1998\)002<0001:TOOTTS>2.3.CO;2](https://doi.org/10.1175/1087-3562(1998)002<0001:TOOTTS>2.3.CO;2)
- Göögüs, O. (2015). Rifting and subsidence following lithospheric removal in continental back arcs. *Geology*, 43(1), 3–6. <https://doi.org/10.1130/G36305.1>
- Higgins, K., Hashimoto, T., Rollet, N., Colwell, J., Hackney, R., & Milligan, P. (2015). Structural analysis of extended Australian continental crust: Capel and Faust basins, Lord Howe rise. *Geological Society, London, Special Publications*, 413(1), 9–33. <https://doi.org/10.1144/SP413.6>
- Hopper, J. R., Dahl-Jensen, T., Holbrook, W. S., Larsen, H. C., Lizarralde, D., Korenaga, J., et al. (2003). Structure of the SE Greenland margin from seismic reflection and refraction data: Implications for nascent spreading center subsidence and asymmetric crustal accretion during North Atlantic opening. *Journal of Geophysical Research*, 108(B5), 2269. <https://doi.org/10.1029/2002JB001996>
- Jongsma, D., & Mutter, J. C. (1978). Non-axial breaching of a rift valley: Evidence from the Lord Howe Rise and the southeastern Australian margin. *Earth and Planetary Science Letters*, 39(2), 226–234. [https://doi.org/10.1016/0012-821X\(78\)90198-X](https://doi.org/10.1016/0012-821X(78)90198-X)
- Klingelhoefer, F., Evain, M., Afilhado, A., Rigoti, C., Loureiro, A., Alves, D., et al. (2014). Imaging proto-oceanic crust off the Brazilian Continental Margin. *Geophysical Journal International*, 200(1), 471–488. <https://doi.org/10.1093/gji/ggu387>
- Klingelhoefer, F., Lafay, Y., Collot, J., Cosquer, E., Géli, L., Nouzé, H., & Vially, R. (2007). Crustal structure of the basin and ridge system west of New Caledonia (southwest Pacific) from wide-angle and reflection seismic data. *Journal of Geophysical Research*, 112, B11102. <https://doi.org/10.1029/2007JB005093>
- Klingelhöfer, F., Edwards, R. A., Hobbs, R. W., & England, R. W. (2005). Crustal structure of the NE Rockall Trough from wide-angle seismic data modeling. *Journal of Geophysical Research*, 110, B11105. <https://doi.org/10.1029/2005JB003763>
- Kodaira, S., Fujie, G., Yamashita, M., Sato, T., Takahashi, T., & Takahashi, N. (2014). Seismological evidence of mantle flow driving plate motions at a palaeo-spreading Centre. *Nature Geoscience*, 7(5), 371–375. <https://doi.org/10.1038/ngeo2121>
- Kodaira, S., Mjelde, R., Gunnarsson, K., Shiobara, H., & Shimamura, H. (1998). Structure of the Jan Mayen microcontinent and implications for its evolution. *Geophysical Journal International*, 132, 383–400.
- Lavier, L. L., & Manatschal, G. (2006). A mechanism to thin the continental lithosphere at magma-poor margins. *Nature*, 440(7082), 324–328. <https://doi.org/10.1038/nature04608>
- Li, P. F., Rosenbaum, G., & Rubatto, D. (2012). Triassic asymmetric subduction rollback in the southern New England Orogen (eastern Australia): The end of the Hunter-Bowen Orogeny. *Australian Journal of Earth Sciences*, 59(6), 965–981. <https://doi.org/10.1080/08120099.2012.696556>
- Lister, G. S., Etheridge, M. A., & Symonds, P. A. (1986). Detachment faulting and the evolution of passive continental margins. *Geology*, 14(3), 246–250.
- Lister, G. S., Etheridge, M. A., & Symonds, P. A. (1991). Detachment models for the formation of continental margins. *Tectonics*, 10(5), 1038–1064. <https://doi.org/10.1029/90TC01007>
- Matthews, K. J., Williams, S. E., Whittaker, J. M., Müller, R. D., Seton, M., & Clarke, G. L. (2015). Geologic and kinematic constraints on Late Cretaceous to mid Eocene plate boundaries in the southwest Pacific. *Earth-Science Reviews*, 140, 72–107. <https://doi.org/10.1016/j.earscirev.2014.10.008>
- McDougall, I., & Duncan, A. R. (1988). Age progressive volcanism in the Tasmantid Seamounts. *Earth and Planetary Science Letters*, 89(2), 207–220. [https://doi.org/10.1016/0012-821X\(88\)90173-2](https://doi.org/10.1016/0012-821X(88)90173-2)
- McDougall, I., Maboko, M. A. H., Symonds, P. A., McCulloch, M. T., Williams, I. S., & Kudrass, H. R. (1994). Dampier Ridge, Tasman Sea as a stranded continental fragment. *Australian Journal of Earth Sciences*, 41(5), 395–406. <https://doi.org/10.1080/08120099408728150>
- Mittelstaedt, E., Ito, G., & Behn, M. D. (2008). Mid-ocean ridge jumps associated with hotspot magmatism. *Earth and Planetary Science Letters*, 266(3–4), 256–270. <https://doi.org/10.1016/j.epsl.2007.10.055>
- Molnar, N. E., Cruden, A. R., & Betts, P. G. (2018). Unzipping continents and the birth of microcontinents. *Geology*, 46(5), 451–454. <https://doi.org/10.1130/G40021.1>
- Mortimer, N., Gans, P. B., Meffre, S., Martin, C. E., Seton, M., Williams, S., et al. (2018). Regional volcanism of northern Zealandia: Post-Gondwana break-up magmatism on an extended, submerged continent. *Geological Society of London, Special Publication*, 463(1), 199–226. <https://doi.org/10.1144/SP463.9>
- Mortimer, N., Turnbull, R. E., Palin, J. M., Tulloch, A. J., Rollet, N., & Hashimoto, T. (2015). Triassic–Jurassic granites on the Lord Howe Rise, northern Zealandia. *Australian Journal of Earth Sciences*, 62(6), 735–742.
- Mortimer, N., Campbell, H. J., Tulloch, A. J., King, P. R., Stagpoole, V. M., Wood, R. A., et al. (2017). Zealandia: Earth's hidden continent. *GSA Today*, 27–35. <https://doi.org/10.1130/GSATG321A.1>
- Müller, R. D., Flament, N., Matthews, K. J., Williams, S. E., & Gurnis, M. (2016). Formation of Australian continental margin highlands driven by plate–mantle interaction. *Earth and Planetary Science Letters*, 441, 60–70. <https://doi.org/10.1016/j.epsl.2016.02.025>
- Müller, R. D., Gaina, C., Roest, W. R., & Lundbek Hansen, D. (2001). A recipe for microcontinent formation. *Geology*, 29(3), 203–206. [https://doi.org/10.1130/0091-7613\(2001\)029<0001:ARFMF>2.0.CO;2](https://doi.org/10.1130/0091-7613(2001)029<0001:ARFMF>2.0.CO;2)
- Müller, R. D., Sdrolias, M., Gaina, C., & Roest, W. R. (2008). Age, spreading rates, and spreading asymmetry of the world's ocean crust. *Geochemistry, Geophysics, Geosystems*, 9, Q04006. <https://doi.org/10.1029/2007GC001743>
- Mutter, J. C., Buck, W. R., & Zehnder, C. M. (1988). Convective partial melting: 1. A model for the formation of thick basaltic sequences during the initiation of spreading. *Journal of Geophysical Research*, 93(B2), 1031–1048. <https://doi.org/10.1029/JB093iB02p01031>

- Pérez-Gussinyé, M., & Reston, T. J. (2001). Rheological evolution during extension at nonvolcanic rifted margins: Onset of serpentinization and development of detachments leading to continental breakup. *Journal of Geophysical Research*, 106(B3), 3961–3975. <https://doi.org/10.1029/2000JB900325>
- Pichot, T., Delescluse, M., Chamot-Rooke, N., Pubellier, M., Qiu, Y., Meresse, F., et al. (2014). Deep crustal structure of the conjugate margins of the SW South China Sea from wide-angle refraction seismic data. *Marine and Petroleum Geology*, 58, 627–643. <https://doi.org/10.1016/j.marpetgeo.2013.10.008>
- Qiu, X., Ye, S., Wu, S., Shi, X., Zhou, D., Xia, K., & Flueh, E. R. (2001). Crustal structure across the Xisha Trough, northwestern South China Sea. *Tectonophysics*, 341(1–4), 179–193. [https://doi.org/10.1016/S0040-1951\(01\)00222-0](https://doi.org/10.1016/S0040-1951(01)00222-0)
- Reston, T. J. (2009). The structure, evolution and symmetry of the magma-poor rifted margins of the North and Central Atlantic: A synthesis. *Tectonophysics*, 468(1–4), 6–27. <https://doi.org/10.1016/j.tecto.2008.09.002>
- Rey, F. F., & Müller, R. D. (2010). Fragmentation of active continental plate margins owing to the buoyancy of the mantle wedge. *Nature Geoscience*, 3(4), 257–261. <https://doi.org/10.1038/ngeo825>
- Schellart, W. P., Lister, G. S., & Toy, V. G. (2006). A Late Cretaceous and Cenozoic reconstruction of the Southwest Pacific region: Tectonics controlled by subduction and slab rollback processes. *Earth-Science Reviews*, 76(3–4), 191–233. <https://doi.org/10.1016/j.earscirev.2006.01.002>
- Shor, G. G., Kirk, H. K., & Menard, H. W. (1976). Crustal structure of the Melanesian area. *Journal of Geophysical Research*, 76(11), 2562–2586. <https://doi.org/10.1029/JB076i011p02562>
- Stagg, H. M. J., Alcock, M. B., Borissova, I., & Moore, A. M. G. (2002). Geological framework of the southern Lord Howe Rise and adjacent areas. *Geoscience Australia Record*, 2002/25.
- Stagg, H. M. J., Borissova, I., Alcock, M., & Moore, A. M. G. (1999). Tectonic provinces of the Lord Howe Rise. “Law of the Sea” study has implications for frontier hydrocarbons. *AGSO Research Newsletter*, 31.
- Sun, W., & Kennett, B. L. N. (2016). Uppermost mantle structure of the Australian continent from Pn traveltome tomography. *Journal of Geophysical Research: Solid Earth*, 121, 2004–2019. <https://doi.org/10.1002/2015JB012597>
- Sutherland, F., & Fanning, C. M. (2001). Gem-bearing basaltic volcanism, Barrington New South Whales: Cenozoic evolution, based on basalt K-Ar ages and zircon fission track and U-Pb dating. *Australian Journal of Earth Sciences*, 32(1), 89–118. <https://doi.org/10.1144/SP321.5>
- Sutherland, R., Collot, J., Lafoy, Y., Logan, G. A., Hackney, R., Stagpoole, V., et al. (2010). Lithosphere delamination with foundering of lower crust and mantle caused permanent subsidence of New Caledonia Trough and transient uplift of Lord Howe rise during Eocene and Oligocene initiation of Tonga-Kermadec subduction, western Pacific. *Tectonics*, 29, TC2004. <https://doi.org/10.1029/2009TC002476>
- Tulloch, A. J., & Kimbrough, D. L. (1989). The Paparoa Metamorphic Core Complex, New Zealand: Cretaceous extension associated with fragmentation of the Pacific margin of Gondwana. *Tectonics*, 8(6), 1217–1234.
- Tulloch, A. J., Ramezani, J., Mortimer, N., Mortensen, J., van den Bogaard, P., & Maas, R. (2009). Cretaceous felsic volcanism in New Zealand and Lord Howe Rise (Zealandia) as a precursor to final Gondwana break-up. *Geological Society, London, Special Publications*, 321(1), 89–118. <https://doi.org/10.1144/SP321.5>
- van de Beuker, S., Stagg, H. M. J., Sayers, J., Willcox, J. B., & Symonds, P. A. (2003). Geological framework of the Northern Lord Howe Rise and adjacent areas. *Geosci. Aust. Rec.*, 2003/01, 1–116.
- Wessel, P., & Smith, W. H. F. (1998). New, improved version of generic mapping tools released. *Eos, Transactions American Geophysical Union*, 79(47), 579–579. <https://doi.org/10.1029/98EO000426>
- White, R. S., McKenzie, D., & O’Nions, R. K. (1992). Oceanic crustal thickness from seismic measurements and rare Earth element inversions. *Journal of Geophysical Research*, 97(B13), 19,683–19,715. <https://doi.org/10.1029/92JB01749>
- White, R. S., Spence, G. D., Fowler, S. R., McKenzie, D. P., Westbrook, G. K., & Bowen, A. N. (1987). Magmatism at rifted continental margins. *Nature*, 330(6147), 439–444. <https://doi.org/10.1038/330439a0>
- Whitmarsh, R. B., Manatschal, G., & Minshull, T. A. (2001). Evolution of magma-poor continental margins from rifting to seafloor spreading. *Nature*, 413(6852), 150–154. <https://doi.org/10.1038/35093085>
- Willcox, J. B., Sayers, J., Stagg, H. M. J., & van de Beuker, S. (2001). Geological framework of the Lord Howe Rise and adjacent ocean basins. Special Publication. In K. C. Hill & T. Bernecker (Eds.), *Eastern Australasian Basin Symposium, A Refocused Energy Perspective for the Future* (pp. 211–225). Melbourne: Petroleum Exploration Society of Australia.